

N69-40090
CR-106346



CASE FILE
COPY

Bellcomm, Inc.

Bellcomm, Inc.

Washington, D. C. 20024

TR-69-235-1

A MODEL OF THE MARTIAN HAZE

July 14, 1969

E. N. Shipley

Work performed for Manned Space Flight, National Aeronautics and
Space Administration under Contract NASW-417.

TABLE OF CONTENTS

ABSTRACT

1.0 INTRODUCTION

2.0 DESCRIPTION OF THE HAZE MODEL

2.1 DISTRIBUTION OF THE HAZE

2.2 THE SCATTERING PROCESS

2.3 NUMERICAL VALUES

2.4 DUST MODEL

3.0 PARAMETER STUDY

3.1 ATMOSPHERIC BRIGHTNESS

3.2 SLOPE SENSITIVITY

3.3 OVERALL BRIGHTNESS AND THE DISCONTINUITY OF THE LIMB

3.4 CONCLUSION

4.0 ACCURACY OF THE COMPUTATIONS

5.0 BRIGHTNESS CALCULATIONS

6.0 CONCLUSIONS

APPENDIX A

APPENDIX B

ABSTRACT

The pictures of Mars returned to Earth by the Mariner IV spacecraft revealed two anomalies. First, there was a region of brightness extending to at least 150 km above the limb of the planet, and second, the contrast in the pictures was surprisingly low. Both of these results can be explained by the presence of a haze surrounding the planet. However, it is possible that the anomalies arose from an abnormal condition in the spacecraft camera system.

A haze model which explains the results of Mariner IV is presented in some detail. The brightness calculations are made on the basis of a first-order scattering theory. The parameters describing the haze cannot be uniquely determined from the data. However, a wide range of parameters provide a reasonable fit to the data. An adopted set of parameters was chosen for further study of the brightness distributions near the planet.

The accuracy of the first order scattering approximation was checked by comparing the results to multiple scattering calculations for the specific case of a planar atmosphere. The first-order theory gives brightnesses which are typically 25% low, but it preserves the shape of the dependence on the viewing angle. It is expected that because of the reasonably good results, the first order theory may be useful as a starting point for calculations to a higher approximation.

The brightness of the planet, including the haze, was calculated for a wide range of geometries to provide data for mission planning purposes. The calculated phase function of the planet closely resembles that obtained from a Lambert surface, which was used to represent the planet surface. This is inconsistent with earth-based observations and indicates that a more accurate description of the surface photometry will eventually be required.

The most significant result of the haze model is that it is able to explain both the brightness above the limb and the low surface contrast seen by Mariner IV through a single model. In order to obtain high accuracy for the calculated brightness, multiple scattering effects must be included, and the effect of the gaseous atmosphere of the planet must be taken into account.

A MODEL OF THE MARTIAN HAZE

1.0 INTRODUCTION

In July of 1965, Mariner IV obtained close-up photographs of the planet Mars. The pictures were subsequently telemetered to Earth and reconstructed. A considerable advance in the knowledge of the topography of the planet, and of the processes which shape the surface, has been gained from the analysis of the pictures.

However, the photometric results from the pictures were surprising, and perhaps disappointing, for two reasons. First, the contrast in the pictures, or the brightness variations from which one determines the shapes of the features on the surface, was very low, even for a planet known to have low contrast from earth-based observations. It should be noted, however, that because of the difference in resolution, contrast as seen from the Earth corresponds to albedo differences between various terrain units on the surface of the planet, whereas the little contrast that was observed by Mariner IV arose principally from the brightness differences due to slope changes. Thus, earth-based contrast is not directly comparable to that observed by Mariner IV.

The second surprising photometric result was the extensive brightness detected in the atmosphere above the limb of the planet. The first photograph taken by Mariner IV included the limb of the planet and the region above the limb to an altitude of about 150 km. The entire region above the limb was essentially uniformly bright.

This brightness cannot be accounted for by Rayleigh scattering from the gaseous atmosphere of Mars. This conclusion rests principally on the great height to which the brightness extends. Present models of the Mars atmosphere give brightnesses comparable to that observed by Mariner IV, but only to altitudes of 5 or 10 km. ⁽¹⁾ At altitudes above 50 km, the gaseous atmosphere becomes so tenuous that the brightness which would be produced is no longer comparable to that measured by Mariner IV.

There are two hypotheses relating to this situation: either the brightness above the limb and the low contrast in the pictures are real effects whose explanation lies in the physical properties of Mars, or both photometric effects are to be ascribed, at least in part, to some failing in the camera system for Mariner IV.

Considerable effort has been expended to attempt to resolve this question. (2) It is the opinion of the television experimenters for the Mariner IV mission that the observed effects must arise at least partially from a real haze. They reach this conclusion because there was no apparent camera failure, including such things as glare and fogging of the optics, which could produce the effect in the photographs from Mariner IV.

It should be understood that at this time the acceptance of the effects as real is a matter of judgment. There is no conclusive answer one way or the other, and a definitive resolution of these questions must await further data.

The subject of this report is a model of a haze surrounding Mars. The model was developed explicitly to explain the photometric phenomena of Mariner IV. The model provides a quantitative explanation for both the brightness above the limb and for the low contrast observed in all of the Mariner IV pictures. The agreement between the results of the model and the observational data from Mariner has been described previously. (3)

The model presented in this report consists of three basic parts: a spatial distribution of haze surrounding the planet, an approximate differential equation which relates the haze density to the brightness seen by the detector, and a set of digital computer programs which integrate the differential equation for the desired geometric relationship among detector, planet and Sun. A detailed discussion of the computer programs is not included in this report.

The purpose of this report is three-fold. First, as a matter of future reference, it is desired to describe the model in some detail, so that the model itself, the approximations which are made, the basis for the choice of haze distributions, and the capabilities of the model are readily available. Second, brightness calculations and other photometric properties of planet, as computed through the model, are presented for a wide range of geometries. The purpose here is to examine the consequences of the theory in order to check their compatibility with earth-based data, to establish a basis for comparison with the data from Mariner '69, and to provide data for mission planning for Mariner '71.* The third purpose is to present calculations which indicate the accuracy of the approximations used in the model.

*The author is a member of the Photointerpretation Team for the 1971 Mariner Mars orbiter mission.

This work is in the nature of a status report. A haze model has been developed which is in reasonable agreement with Mariner IV data. However, certain approximations and simplifying assumptions have been made which limit the accuracy of the calculations. It is expected that new data, obtained from Mariner '69 and Mariner '71, will reveal inconsistencies with the present model. Although the model is adequate for its initial intended use, the inherent limitations restrict its validity and generality. It is well to pause and consider the model in detail, and to bring its deficiencies into sharper focus, so as to indicate where improvements are desirable.

2.0 DESCRIPTION OF THE HAZE MODEL

2.1 Distribution of the Haze

The haze is described in terms of its physical effects on the transmission of light rather than in terms of a spatial distribution of scatterers. It may reasonably be hoped that, given sufficient data, a unique description of the haze in terms of its physical properties will be found. A subsequent step, not considered in this report, is to deduce a distribution of scatterers which is based on planetary processes and which is compatible with the physical properties of the haze.

In moving through the haze, light is both absorbed and scattered. The extinction coefficient, σ , determines the fractional part of a beam of light that is removed per unit length

$$\frac{d\omega}{d\chi} = -\sigma\omega \quad (1)$$

where ω is the intensity of the beam (lumens per unit area and solid angle) and χ is the distance measured parallel to the beam. The extinction coefficient includes both the effects of scattering and of absorption.

The extinction coefficient is assumed to have an exponential dependence on altitude above the surface

$$\sigma = \sigma_0 e^{-h/h_0} \quad (2)$$

where h is the height above the surface, h_0 is the scale height

and σ_0 is the value of the extinction coefficient extrapolated to zero altitude. However, the haze does not in general extend from the surface to an arbitrarily great altitude, but is bounded by a low altitude cutoff h_{CO} and a high altitude cutoff h_{max} . The extinction coefficient is non-zero only for the interval

$$h_{CO} \leq h \leq h_{max}$$

The value of the extinction coefficient is illustrated in Figure 1.

The high altitude cutoff is used only for convenience in order to have a specific point at which to start the integration of the differential equations. It is chosen sufficiently high that any change in h_{max} has no appreciable effect on the brightness calculations.

On the other hand, the low altitude cutoff, h_{CO} , is a very important parameter whose adjustment significantly affects the agreement between the model and the data from Mariner IV. Without the use of a low altitude cutoff, hazes adequate to explain the lack of contrast in the Mariner pictures would completely obscure the limb of the planet, which, however, is distinctly visible in the first photograph. The removal of haze near the surface affects the lines of sight passing near the limb to a much greater extent than those which represent normal viewing of the surface.

The data from Mariner IV are inadequate to distinguish the exponential haze profile, which has been used here, from other possible distributions. When one is dealing with a spherical geometry, the profile of the haze can make a difference in the observed brightness. It will be shown later that the effect is particularly strong in certain specific regions, such as near the terminator, where the shadow cast by the planet progressively shields higher altitudes from the solar illumination. Consequently, pictures taken near the terminator may provide a sensitive indicator of the vertical structure of the atmosphere.* This point deserves emphasis because for a flat atmosphere, for which most atmospheric scattering work has been done, the brightness does not depend on the profile, but only the total optical thickness of the layer.⁽⁴⁾ The sensitivity to profile is a bonus of the spherical geometry.

*It is expected that such pictures will be taken by the Mariner '71 spacecraft.

In addition to the haze distribution, it is necessary to describe the reflective properties of the planet itself if one is to calculate the brightness to be expected in pictures containing the surface. We have chosen to represent the Martian surface as a diffuse scatterer (Lambert surface) with an albedo ρ . This choice was made because the brightness of a Lambert surface depends only on the incident flux and not on the direction from which the radiation is incident, and this provides a significant simplification in calculating the effect of skylight on the surface. Although the choice was made for convenience, there are no data available to provide a more accurate description of the surface reflective properties.

2.2 The Scattering Process

When light interacts with a scattering particle, some of the light is scattered and the remainder is absorbed by the scattering particle. The ratio of the scattered light to the total light removed from the incident beam is termed the albedo for a single particle scattering, ρ_s .

In order to describe the scattering process completely, it is necessary to give the angular distribution of the radiation scattered from a point. Scattering theory is well developed⁽⁵⁾ for molecules small in size compared to the wavelength of light (Rayleigh scattering) and for dielectric spheres (Mie scattering). These theories predict the extinction coefficient and the angular distribution of the scattered radiation in terms of the size, shape and dielectric properties of the scattering medium.

In the case of the haze with which we are dealing here, the physical properties are not known a priori, so one would have to guess at the angular distribution. Again on the basis of simplicity in the calculations, isotropic scattering has been chosen. The observed brightness is not independent of this choice. For example, Rayleigh scattering for unpolarized light differs by a factor of two between the maximum and minimum intensities as a function of direction, and its use would cause a variation in the brightness as a function of viewing geometry. It may be possible to obtain information on the scattering function of the haze by observing the brightness of the region above the limb at different phase angles. No such data are available from Mariner IV.

The scattering coefficient, b , is the fraction of the incident beam which is scattered (as opposed to being absorbed), and is related to the extinction coefficient σ through the relation

$$b = \rho_s \sigma \quad (3)$$

This definition of b is most useful in the case of isotropic scattering. Slightly different definitions have been used for other scattering laws. (1)

The apparent brightness, ω , seen by a detector obeys the relation

$$\frac{d\omega}{d\chi} = -\sigma\omega + \frac{b}{4} e^{-\tau_s(\chi)} + \frac{bU}{4} \quad (4)$$

where $\tau_s(\chi)$ is the optical thickness of the haze between the source of the incident radiation (the Sun) and the point χ which lies along the line of sight of the detector. U is the integrated intensity of radiation, excluding the incident source radiation, arriving at the point χ . The derivation of Equation 4 and the initial values utilized in its solution are given in Appendix A.

In Equation 4, and in the remainder of this report, the brightness is always given as the ratio of the observed brightness to the brightness of an ideal Lambert surface oriented normally to the incident solar radiation. We have used the term millilamb, where 1000 millilambs correspond to a ratio of unity between the apparent brightness and the brightness of the Lambert surface.

The last term in Equation 4 accounts for multiple scattering. It represents the scattering, at the point χ , of light which has already been scattered at least once within the atmosphere, or which has been reflected from the surface of the planet. For the first-order theory, which is the topic of this report, we consider only the first scattering of the incident solar radiation, and hence we take

$$U = 0 \quad (5)$$

In a real physical situation, U must always be greater than or equal to 0. Thus, setting U equal to 0 must decrease the value of ω obtained as a solution of Equation 4. The first-order theory of necessity underestimates the brightness. The degree to which it does this depends on the optical thickness of the atmosphere. This question will be discussed in Section 4.0.

The surface brightness is easily calculated once the surface illumination has been determined. In most circumstances, the principal source of illumination is the incident solar radiation. In addition, however, light scattered from the atmosphere contributes to the surface illumination, and near the

terminator this "skylight" becomes the dominant source of illumination. In the haze model, the skylight is calculated to the same first-order scattering approximation that is used elsewhere.

2.3 Numerical Values

The numerical values for the parameters of the haze model are given in Table I. These represent an adopted set of values in that the data of Mariner IV may be explained by a wide range of values for each of the parameters. A single set of parameters was adopted in order that we can be specific in the brightness calculations presented in subsequent sections. The range of values over which the parameters could have been chosen is discussed in detail in Section 3.0.

The principal motivation behind the choice of the adopted set of parameters was the selection of a scale height similar to that which has been estimated for the Martian gaseous atmosphere.⁽⁶⁾ However, no mechanism relating the gaseous atmosphere to the haze is proposed in this report.

2.4 Dust Model

The haze model as set forth above is a description of the manner in which the haze interacts with the light. A reasonable question to ask at this point is what phenomena could give rise to the postulated haze. An entirely rational account would take into account the physical processes of the planet to devise a possible mechanism. Such a discussion of planetary processes is not included in this report.

However, we can determine a distribution of scatterers which would have the required photometric properties. The primary information which can be developed from the Mariner IV data is the photometric properties of the haze. The distribution of scatterers is intended to provide an indication of density of material required to achieve the observed photometric properties. The density of material depends on the nature of the scatterers, and in this example, the simplest possible assumptions have been made. Suppose the scatterers consist of spherical dust particles 10 microns in diameter. The angular distribution of the scattered light would be isotropic if the light were scattered specularly from the surface. It is assumed that one half of the radiation incident on the sphere would be scattered and the remainder absorbed.

The size of the particles was chosen so that diffraction scattering can be ignored. For particles large compared to the wavelength of light, the diffracted light is scattered so nearly forward as to be indistinguishable from the original beam.

For light of wavelength 0.5 microns and for the particle size used here, the diffracted light is contained within a cone whose half-angle is roughly 3° . The magnitude of diffracted light can be appreciable. In the case of Mie scattering for large particles, the effect increases the scattering cross section by a factor of two above the geometric area of the scattering particle. ⁽⁵⁾

Since the diffraction effects are neglected, the scattering cross section is equal to the geometric cross section of the particles, and the required density of particles to produce the extinction coefficient for the haze model shown in Figure 1 may be easily calculated. The required density is plotted in Figure 2. The maximum density is 0.5 particles/cm³, which is a very large density. However, the average density in the region in which the haze exists is only 0.06 particles/cm³.

3.0 PARAMETER STUDY

The parameter study represents a specific effort to find a set of parameters for which the calculated brightnesses agree reasonably well with the Mariner IV data and which seem physically reasonable. The process is at least partly subjective. Since no model of a physical process to produce the haze has been put forward, there is no specific test of reasonableness. Moreover, certain parameters can be varied over a wide range without varying significantly the agreement with the data.

The purpose here is not to demonstrate agreement with the Mariner IV data, but rather to provide further insight into the model. It is hoped that such insight may provide a feeling for the flexibility of the model and for the measurements to which it is most sensitive. Because of this, the main attention will be focused on the objective considerations in the choice of parameters.

3.1 Atmospheric Brightness

The first Mariner IV picture revealed a bright sky extending to at least 150 km above the surface of the planet. The observed brightness above the limb may be seen in Figure 12, which will be discussed in more detail subsequently. The measured brightness is not completely uniform since there is some increase in brightness at low altitudes. It is quite possible that this arises from scattering in the gaseous atmosphere of the planet, an effect which has not yet been included in the haze model. Consequently, the shape of the brightness profile was not considered in detail.

Instead, it was assumed that the haze produced an essentially uniform brightness out to about 150 km. If the brightness extended a significant distance beyond 150 km, it surely would give rise to obvious effects in earth-based observations. Therefore, the brightness of the haze must decrease rapidly above an altitude of 150 km.

The principal parameters which affect the calculated brightness above the limb are the scale height, h_0 , extinction coefficient, σ_0 , and the albedo for single scattering, ρ_s . For a fixed scale height and albedo for single scattering, Figure 3 shows how a change in the extinction coefficient changes the altitude to which the haze extends. These calculations were made for the geometry corresponding to that seen by Mariner IV. The brightness is proportional to ρ_s , so that it is easy to adjust the haze model to give the desired brightness above the limb. A value of 100 millilambs was taken as the goal.

The behavior of the brightness profile may be understood qualitatively as follows. Starting at very high altitudes, the haze is very tenuous and the brightness is low. As one looks closer to the limb, the density of the haze increases as does the observed brightness. A critical point is reached when the optical thickness along the line of sight reaches about unity, since such an optical depth represents, in a rough sense, the maximum distance which light can move through the atmosphere. As the observer looks still closer to the limb, he does not receive contributions from the entire line of sight, but only from that which is within one optical depth. The increasing density of the haze at lower altitudes does not increase the brightness seen by the observer but limits the region of the atmosphere which produces a measurable effect at the observer's vantage point. Thus structure deep within the atmosphere, specifically the existence of a low altitude cutoff, does not produce an effect on the brightness profile.

It is clear from Figure 3 that the altitude at which the brightness begins to decrease sharply can be determined by the proper choice of σ_0 . Indeed, for any scale height, one can find a value of σ_0 such that the brightness extends to the desired altitude and then begins to decrease. The minimum value of σ_0 which extends the brightness to 150 km is plotted in Figure 4 as a function of the scale height. The specific criterion used to select the minimum value of σ_0 was that the brightness at 150 km be 75% of the maximum calculated brightness above the limb.

For altitudes below 150 km, the brightness profile for the larger scale heights is in all respects similar to that shown in Figure 3. Above 150 km, larger scale heights cause the decrease in brightness to be more gradual, and in fact the rate of decrease of the brightness at high altitudes is a measure of the scale height. The desire to have a rapid decrease in the brightness above 150 km, in order to avoid conflict with earth-based data, suggests that a small scale height be chosen.

There is no reason to rule out higher than minimum values of σ_0 . Their use merely extends to a higher altitude the region in which the brightness is essentially constant, without affecting the brightness profile at lower levels.

3.2 Slope Sensitivity

The topography of a surface is revealed by brightness changes which arise due to the different sun-surface-viewer geometry of the various slopes. The ability to perceive a specific feature on the surface depends on the photometric properties of the surface, the viewing geometry, and the characteristics of the detector, a camera in the case of Mariner IV. In addition, the presence of haze between the camera and the surface will affect the detection of the topographic features.

The Mariner IV pictures had unexpectedly low contrast. Enhancement of the contrast is necessary to make the features obvious in the reproductions of the pictures. One does not know the photometric properties of Mars, so it is not possible to decide if the origin of the low contrast lies in the properties of the surface, a defect in the camera, or in the presence of haze.

However, the variation in contrast as the trajectory of Mariner IV brought about changes in the viewing geometry provides useful data. Instead of the contrast itself, we use the ability to detect topographic features as a measure of the contrast, or more specifically, the slope sensitivity. Slope sensitivity, as defined here, means the change in brightness produced by a change in the slope of a surface. Where the slope sensitivity is high, features with gentle slopes may be detected, while if the slope sensitivity is low, greater slopes are required to produce brightness changes which are adequate to be detected.

The slope sensitivity depends on the photometric properties of the surface and on the characteristics of the haze. Ignoring the haze for a moment, a general property of the slope

sensitivity, valid certainly for ordinary photometric surfaces, is that the slope sensitivity is greatest when the sun incidence angle is near 90°, that is, near the terminator. This property is valid for the moon and for Lambert surfaces.

Figure 5 shows the number of detectable craters seen in each pair of Mariner IV pictures. There is clearly a peak in the vicinity of picture pair 9-10, with a significantly smaller number of craters detected on both sides of the maximum. The viewing geometry under which the pictures were taken is shown in Figure 6. The Sun angle, which is measured from local vertical, increases from Pictures 4 to 22; Picture 19 is near the terminator. The viewing angle, which is measured from the local vertical to the line of sight, goes through a pronounced minimum in the vicinity of Picture 11.

It is clear that the number of craters detected per picture pair deviates from what is expected on the basis of the simple slope sensitivity argument. Instead of an increasing number of craters near the terminator, corresponding to an increase in the slope sensitivity, there is a distinct decrease.

It has been shown⁽³⁾ that this decrease cannot be accounted for by either changes in topography or in the camera-to-surface distance. The falloff in crater counts for the later pictures can be accounted for by a reduction in the slope sensitivity caused by the haze. To see this, it is first necessary to define the slope sensitivity in mathematical terms. Consider a reference surface whose normal lies along the local vertical. Suppose the normal to the reference surface is tilted away from vertical by a small angle k in an azimuthal direction ω . Then the slope sensitivity μ is given by

$$\mu = \left\langle \left. \left| \frac{\partial B_a}{\partial k} \right| \right|_{k=0} \right\rangle \quad \text{average over } \omega$$

where B_a is the apparent brightness of the surface in the appropriate geometry. For a Lambert surface with no haze, this depends only on the Sun incidence angle.

This definition of slope sensitivity assumes that the eventual observer can detect the same brightness difference independent of the average scene brightness. This was approximately true for Mariner IV where the exposure, iris setting and gain setting remained constant during the major portion of the

picture taking sequence.* Since the data were returned to Earth digitally, the minimum detectable brightness difference corresponds to one digital number. The brightness difference corresponding to one digital number is shown in Figure 7 as a function of digital number. In the Mariner IV pictures, the commonly occurring digital numbers⁽²⁾ lie in the range 15 to 55 in which interval the brightness difference per digital number, and hence the minimum detectable brightness difference, is reasonably constant.

The haze affects the slope sensitivity in two important ways. First, it attenuates the incident sunlight, and second, it attenuates the light scattered back toward the camera. Both of these effects reduce the apparent brightness difference between surfaces having different slopes.

The low altitude cutoff plays a significant role in the shape of the slope sensitivity curve, as is shown in Figure 8. For lower cutoff altitudes, the optical thickness of the atmosphere is greater and there is an overall reduction in slope sensitivity. The effect is more pronounced for high incidence angles (high incidence and high viewing angles coincide; see Figure 6) because at high viewing or incidence angles the line of the Sun or the line of sight has a greater path length at low altitudes than in the case of normal incidence. Therefore the high angle cases are more affected by the change in the low altitude haze.

Curves similar to those of Figure 8 can be developed for any scale height for any value of the extinction coefficient. A minimum and maximum value of the low altitude cutoff for which the shape of the slope sensitivity curve matches qualitatively the measured values (Figure 5) can be determined. These values are plotted in Figure 9 as a function of the scale height for the case where the extinction coefficient is equal to the minimum value appropriate to the scale height and for the case where the extinction coefficient is twice the minimum.

The maximum value of the low altitude cutoff was determined by two requirements.

- a) The calculated slope sensitivity must reach a maximum before Picture 13.
- b) The slope sensitivity for Pictures 1 and 19 must be less than one half the maximum.

*The only change that occurred for Mariner IV was in the gain of the vidicon amplifier. This gain remained the same for Pictures 1 through 18. The crater counts do not extend beyond Picture 16.

Higher cutoffs do not reduce the slope sensitivity adequately to explain the results for the Mariner IV pictures near the terminator.

The minimum value of the low altitude is determined by the requirement that the slope sensitivity exceed a value of 0.04. This criterion was established to insure that the haze was not so dense as to prohibit detecting any features on the surface. However, the value selected (0.04) is quite arbitrary.

The slope sensitivity that arises when the adopted set of parameters is used (see Table I) is shown in Figure 10. The shape of the curve may be compared to the crater counts given in Figure 5. The calculated slope sensitivity has a peak which occurs for somewhat later pictures than the maximum crater count, but otherwise the curves are very similar. The peak of the calculated slope sensitivity could have been shifted to a lower picture number through the choice of a lower cutoff altitude. However, as we will see subsequently, this would alter the calculated brightnesses in other areas.

3.3 Overall Brightness and the Discontinuity at the Limb

There are two remaining types of data which provided some guidance in the choice of the adopted set of parameters. These data are the average brightness in the individual Mariner IV pictures and the brightness discontinuity at the limb.

The results for the average brightness are shown in Figure 11. The measured brightnesses from Mariner IV were corrected for the presence of glare⁽²⁾ in the optical system of the spacecraft. The calculated results were obtained for the adopted set of parameters.

Similar calculated curves can be obtained for any scale height. The principle use of these data is to select the surface albedo of the planet. In general, for a given scale height, the lower the cutoff altitude, the higher the albedo required to match the average brightness. The reason for this is that, as can be seen in Figure 11, the haze contributes little to the scene brightness; its principal effect is to attenuate the light reflected from the planet. Therefore, any change which increases the optical thickness of the haze, such as lowering the cutoff altitude, will necessitate a greater planetary reflectivity to achieve the observed brightness.

Since the required albedos are around 0.5, which seems unusually high, this influences one to choose the highest possible cutoff altitudes.

The detailed shape of the calculated curve (Figure 11) depends on the photometric function of the surface. Deviations of the calculated from the measured brightness may reasonably be attributed to the non-Lambertian character of the surface. It should also be noted that the value chosen for the albedo depends on the photometric function, and the albedo required might be somewhat reduced if an exact photometric function were known.*

The deviations between the measured and calculated brightness represent information from which the photometric function of the planet may be, in part, extracted. The use of the data in this way does not seem warranted at the present time both because the range of incidence and viewing angles is not nearly complete and because of the arbitrariness in the choice of haze parameters. However, the procedure is obvious, and it should be noted that knowledge of the haze is essential in order to obtain precise information on the characteristics of the surface.

Another important source of data is the discontinuity in brightness at the limb of the planet. The reason for the importance of this data, which is shown in Figure 12, is that the brightness of the haze changes very little above and below the limb. Consequently, the discontinuity represents the brightness of the surface attenuated by the haze. It may be seen that for the adopted set of parameters, the discontinuity is obtained correctly, but that the calculated brightness is lower than that measured. Better agreement would be obtained if a higher single scattering albedo were used. This would proportionally increase all of the brightness above the limb and the haze contribution below it, but leave the discontinuity unaffected.

3.4 Conclusion

Considerable variation is possible in the choice of values for the parameters which describe the Martian haze. The set of parameters which has been adopted was chosen from the acceptable range solely on the basis of the judgment of the author. A major judgment was that the scale height of the

*The normal albedo is defined for a specific geometry (normal incidence and viewing angles). In the case of the Mariner IV data, we are choosing an albedo on the basis of average properties over a wide range of geometries.

haze should be comparable to that of the gaseous atmosphere. This was done primarily because it is believed that whatever mechanism is responsible for the haze must be associated with the atmosphere in some way.

Complete agreement between the haze model and the Mariner IV data was not obtained. More precise agreement to specific data could have been obtained with other choices of the parameters, but the adopted set explains all the salient properties of the Mariner IV data, and the discrepancies can be reasonably ascribed to shortcomings which originate in the simplifying assumptions of the haze model.

4.0 ACCURACY OF THE COMPUTATIONS

It appears that the approximation which most seriously restricts the accuracy with which the haze model description is converted to observable brightnesses is the use of a first-order scattering theory. It was indicated in Section 2.0 that higher order scattering was neglected in the calculations, and in this section a quantitative estimate of the error occasioned by the neglect of multiple scattering will be obtained.

The effects of multiple scattering can be taken into account exactly by the use of techniques originated by

Chandrasekhar.⁽⁴⁾ Unfortunately, these methods are useful only for the case of flat atmospheres if, as in our case, there is an external source of radiation. On the other hand, spherical geometry is essential to the haze model since it is necessary to perform calculations near and above the limb.

For the case of normal incidence of the sunlight and normal viewing of the surface, the flat atmosphere case may be a reasonable approximation to the spherical geometry, provided the height of the atmosphere is much less than the radius of curvature of the planet. This situation applies to the haze model, where the maximum height of the atmosphere is 200 km, compared to a radius of curvature which has been taken to be 3360 km.

In order to gain an insight into the accuracy of the calculations, the brightness was calculated in three separate ways. First, the multiple scattering theory of Chandrasekhar was employed for a flat atmosphere. Second, the first-order theory was used to calculate the brightness of the same flat atmosphere, and third, the first-order theory was used to calculate the brightness of the spherical atmosphere which, when viewed along a normal to the surface, matched the flat atmosphere. The low altitude

cutoff was changed slightly from the adopted value given in Table I in order to make the multiple scattering calculation more convenient.*

The solution of the multiple scattering problem is described in more detail in Appendix B. The brightness was calculated for the case where the atmosphere was located above a Lambert surface having an albedo of 0.5. The geometry for this and the other two calculations is shown in Figure 13.

The results of the calculations are shown in Figures 14 through 17, for different Sun incidence angles. In comparing the multiple scattering results with the first-order calculation for a flat atmosphere, it may be seen that the first-order theory is lower, by a substantial percentage, than the multiple scattering results, but that it preserves the shape of the dependence on the look angle. The fact that the first order theory gives a lower result was expected (see Section 2.0) precisely because it neglects multiple scattering. The deviation between these two results shows the accuracy of the first order calculations for the flat atmosphere.

The effect of the spherical geometry can be seen by comparing the first-order calculations for the flat and spherical atmospheres. For normal Sun incidence (Figure 14), the two results agree closely at 0° look angle but diverge as the look angle increases. As the sun angle increases, the results no longer agree even at 0° look angle.

The results for the spherical atmosphere depend on the azimuth angle between the Sun and observer (see Figure 14). The range of variation is shown by cross-hatching in Figures 15 through 17. In all cases, the brightness was greatest for 0° azimuth angle and decreased monotonically as the azimuth angle increased to 180°. For spherically symmetric scattering in a flat atmosphere, there is no azimuthal dependence.

The conclusion which results from the comparison of the single and the multiple scattering results is that multiple scattering must be taken into account if reasonable accuracy (say 3%) is to be achieved. It is encouraging to note, however, that the first-order theory preserves the shape of the brightness curves obtained for multiple scattering in a flat atmosphere, and that the brightness difference caused by the neglect of multiple scattering is reasonably small. These two factors indicate that rapid convergence should be achieved in obtaining multiple scattering results through successive approximations to the first-order theory.

*The low altitude cutoff, h_{CO} , was set equal to 122.3035 km to make the optical thickness of the atmosphere, viewed normally, precisely 0.400. Tabulations of the functions necessary to solve the multiple scattering problem were available for this value.

5.0 BRIGHTNESS CALCULATIONS

The calculated brightnesses presented in this section were all made with the adopted set of parameters given in Table I. The results are presented for essentially a complete range of geometries for the planet and not just for the range of Mariner IV observations. The purpose of presenting these data is to provide a source of information which may be useful for mission planning for forthcoming Mars missions.

The phase function of a planet is the relative brightness of the planet, integrated over the entire disk, as a function of the phase angle (the angle between the Sun, the center of the planet and the observer). The phase function is normalized to unity at zero degrees phase angle. The calculated phase function for Mars is shown in Figure 18, together with the measured phase function of Mars and that which would be observed for a planet with a Lambert surface (and no atmosphere). Because of the geometry relative to the Sun and Earth, the phase function for Mars can be observed only for phase angles less than 48° . The measured and extrapolated values for Mars are those adopted by de Vaucouleurs.⁽⁸⁾

It is clear from Figure 18 that the calculated phase function does not resemble that measured for Mars, and, in fact, deviates only slightly from that for a Lambert surface. That is, the haze has only a small effect on the phase function, which is principally determined by the characteristics of the surface. In order to obtain agreement between the measured and calculated phase function, it will be necessary to describe the surface of the planet by a more appropriate photometric function than a Lambert surface.

The geometric albedo of the planet is the relative brightness of the planet, integrated over the entire disk at zero degrees phase angle, compared to the brightness of an ideal Lambert disc of the same size normal to the Sun and at the same distance to Sun. The measured value, as adopted by de Vaucouleurs from many measurements,⁽⁸⁾ is 0.149. The result calculated from the haze model is 0.164. For the same planetary surface that has been used in the model, but without the haze, the geometric albedo would be 0.333.

The calculated geometric albedo depends on both the haze model and the photometric calibration of the Mariner IV camera system. The haze model was adjusted to give agreement with the photometric results of Mariner IV, and is used to provide brightness values for those geometric configurations not measured by Mariner IV. In turn, the calculated geometric albedo is directly proportional to the photometric calibration of the camera. If the measured brightnesses were higher than the actual

surface brightness, the calculated geometric albedo would be higher than the actual albedo in direct proportion to the calibration error, assuming only that the calibration did not vary during the picture taking sequence. Any disagreement can be attributed to some combination of calibration error and model defect, and correspondingly, the reasonable agreement between the calculated and measured albedos may be taken as providing confidence in the Mariner IV photometric calibration and in the haze model itself.

Figures 19 through 22 are iso-brightness contours for the planet for several different phase angles. It is important to note that these drawings do not represent the projected disc of the planet, but that the data are plotted in a look angle-azimuth angle coordinate system for those regions below the limb of the planet. The principal difference is that the region near the limb is not foreshortened as it is in the case of a simple projected disc. Above the limb of the planet, points are represented by their height above the limb and their azimuth angle in a plane normal to the incident solar radiation. The geometry is shown in Figure 23.

The most interesting feature of the iso-brightness plots is the structure which is apparent near the terminator, especially on the night side. The structure is a direct result of the low altitude cutoff, which allows incident solar rays which just graze the surface of the planet to be less attenuated than parallel rays higher in the atmosphere. This effect, in combination with the shadow pattern of the planet itself, produces the pattern.

The significance of the structure is that it shows the sensitivity of the brightness near the terminator to the detailed structure of the atmosphere. In most geometric situations, the observed brightness results from the cumulative effect of the haze along the entire line of sight, and it is difficult to extract information on the structure of the atmosphere from such data. This is particularly true for a haze of the thickness used in the present model, or for a thicker haze, in which the brightness reaches an equilibrium value in a distance short compared to the total line of sight through the haze. For example, the brightness of the atmosphere away from the terminator shows very little structure below 150 km despite the large variation in the assumed extinction coefficient in this region (see Figure 1).

However, near the terminator the shadow of the planet causes a selective illumination of the high part of the atmosphere in a progressive way as one moves farther to the night side of the terminator. The result is that the atmosphere profile produces a significant effect on the brightness.

A different situation exists when just the gaseous atmosphere of Mars is considered.⁽¹⁾ Because the optical thickness of the atmosphere is not so great as that of the haze model, brightness equilibrium is not achieved along a line of sight through the atmosphere, and the density profile of the atmosphere can be determined by brightness measurements not near the terminator.

It may be noted in Figure 21 that the brightest region of the planet is not at the subsolar point, which for Figure 21 is on the limb (phase angle = 90°). This effect is caused by the attenuation of the haze. Light from the limb travels more obliquely through the atmosphere, and is more attenuated, than light from regions with lower look angles. Consequently the region of greatest brightness is shifted toward lower look angles. The same effect may be noticed to a lesser degree in Figure 20 (phase angle = 45°).

The illumination of the surface is shown in Figure 24. Light scattered from the atmosphere does not play a significant role in surface illumination except near the terminator and towards its dark side. However, skylight illumination exceeding 0.1% of the subsolar illumination extends to Sun angles of 110° , or a distance of almost 1200 km from the night side of the terminator. An observer outside the atmosphere would, however, also see light reflected from the haze. The ability to use the skylight to obtain photographs of the surface region beyond the terminator, either from the surface itself or from outside the atmosphere, depends on the detailed characteristics of the camera.

6.0 CONCLUSIONS

One may conclude that, apart from certain discrepancies arising from detailed assumptions in the haze model, the model which has been described here adequately explains the Mariner IV data and is not inconsistent with earth-based observations. The most significant success of the model is that it can account for both the brightness above the limb and the anomalous behavior of the number of detectable craters, within the framework of a single model. These two observed phenomena, taken together, certainly reinforce one another, and the ability to explain both measurements with a single mechanism is perhaps the strongest reason for accepting the existence of the haze.

The haze model is of course not without difficulties. A prominent one is the high (0.5) surface normal albedo which is required. This is certainly much higher than any familiar surface materials would generate. However, a contributing reason for a high albedo may be our lack of knowledge of the Martian surface photometric function.

Similarly, it is difficult to conceive of a mechanism to generate and maintain so dense a distribution of dust particles as is required by the haze model. This is not a weakness of the model itself, but it may be taken as an argument in favor of the conclusion that some of the measurements derived from the Mariner IV data are erroneous. On the other hand, an exhaustive search for a haze mechanism has not been undertaken.

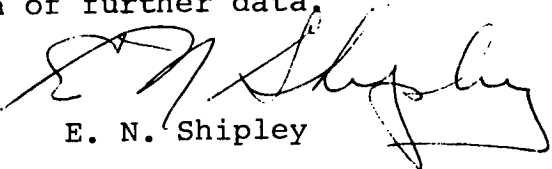
It is also clear that the model itself must be improved in several ways before it can be used to provide a definitive measurement of the Mars environment. The required improvements have been discussed in the previous sections. In order of importance, they are the multiple scattering effect, the inclusion of the gaseous atmosphere, and a better representation of the surface photometry than the presently used Lambert surface.

The surface photometry is accorded least weight because to a large degree the haze itself is independent of the surface. The brightness of the atmosphere above the limb depends in part on the light reflected from the surface, but this effect can be minimized by looking near the terminator where the surface is dark. The principle use of the photometric function is to determine the surface brightness as a function of the lighting and viewing geometry, and this is not a critical aspect of the haze model. Indeed, the photometric function may well be an eventual output of the haze studies.

The use of the first-order theory instead of multiple scattering reduces the intensity by about 25%, so that the inclusion of multiple scattering is obviously necessary to achieve high accuracy. The standard multiple scattering methods are applicable only to flat atmospheres, whereas in our case the spherical atmosphere is of obvious importance. It is expected that multiple scattering for the spherical geometry can be included by a "brute force" method of calculation through the use of a digital computer. Work in this direction appears to have first priority.

In addition, however, the gaseous atmosphere must be included since it can scatter light with the same order of magnitude brightness as does the haze. The total effect should be less because the atmosphere is confined more closely to the surface of the planet.

In summary, a haze model has been set forth which explains to a reasonable degree the data of Mariner IV. There are several directions in which the model must be improved. The question as to whether the haze is real or the data from Mariner IV resulted from anomalous behavior of the camera can only be answered by the acquisition of further data.



E. N. Shipley

1014-ENS-jan

Attachments

Bellcomm, Inc.

Acknowledgement

Mr. G. S. Taylor provided extensive assistance
in preparing the calculations and plots presented in Section 5.0.

REFERENCES

1. E. N. Shipley, "Preliminary Study of the Use of Photographic Measurements of the Atmospheric Brightness of Mars to Study the Atmospheric Structure," Bellcomm, Inc., June 19, 1969.
2. Leighton, Murray, Sharp, Allen and Sloan, "Mariner IV Pictures of Mars," JPL Technical Report 32-884, December 15, 1967.
3. P. L. Chandeysson, E. N. Shipley, and W. B. Thompson, "Haze in the Mars Atmosphere as Revealed by the Mariner IV Television Data," Bellcomm, Inc., TR-68-710-6, August 20, 1968.
4. S. Chandrasekhar, Radiative Transfer, Dover Publications, New York (1960).
5. W. E. K. Middleton, Vision Through the Atmosphere, University of Toronto Press (1952).
6. "Models of Mars Atmosphere," (1967), NASA SP-8010, May 1968.
7. A. H. Marcus, "Number Density of Martian Craters," Bellcomm, Inc., TR-68-710-1, January 20, 1968.
8. G. de Vaucouleurs, Icarus 3, 187 (1964).
9. J. L. Carlstedt and T. W. Mullikin, Ap. J. Suppl., 12, 449 (1966) (No. 113).

TABLE I

The Set of Numerical Values Adopted
For Use in The Haze Model

Scale height, h_0	10 km
Low altitude cutoff, h_{co}	123 km
High altitude cutoff, h_{max}	200 km
Surface normal albedo, ρ	0.5
Extinction coefficient extrapolated to the surface, σ_0	8200/km
Albedo for single particle scattering, ρ_s	0.5
Extinction coefficient $\sigma = \sigma_0 e^{-h/h_0}$	$h_{co} < h < h_{max}$
$\sigma = 0$	$h < h_{co}$
$\sigma = 0$	$h > h_{max}$
Scattering coefficient $b = \rho_s \sigma$	

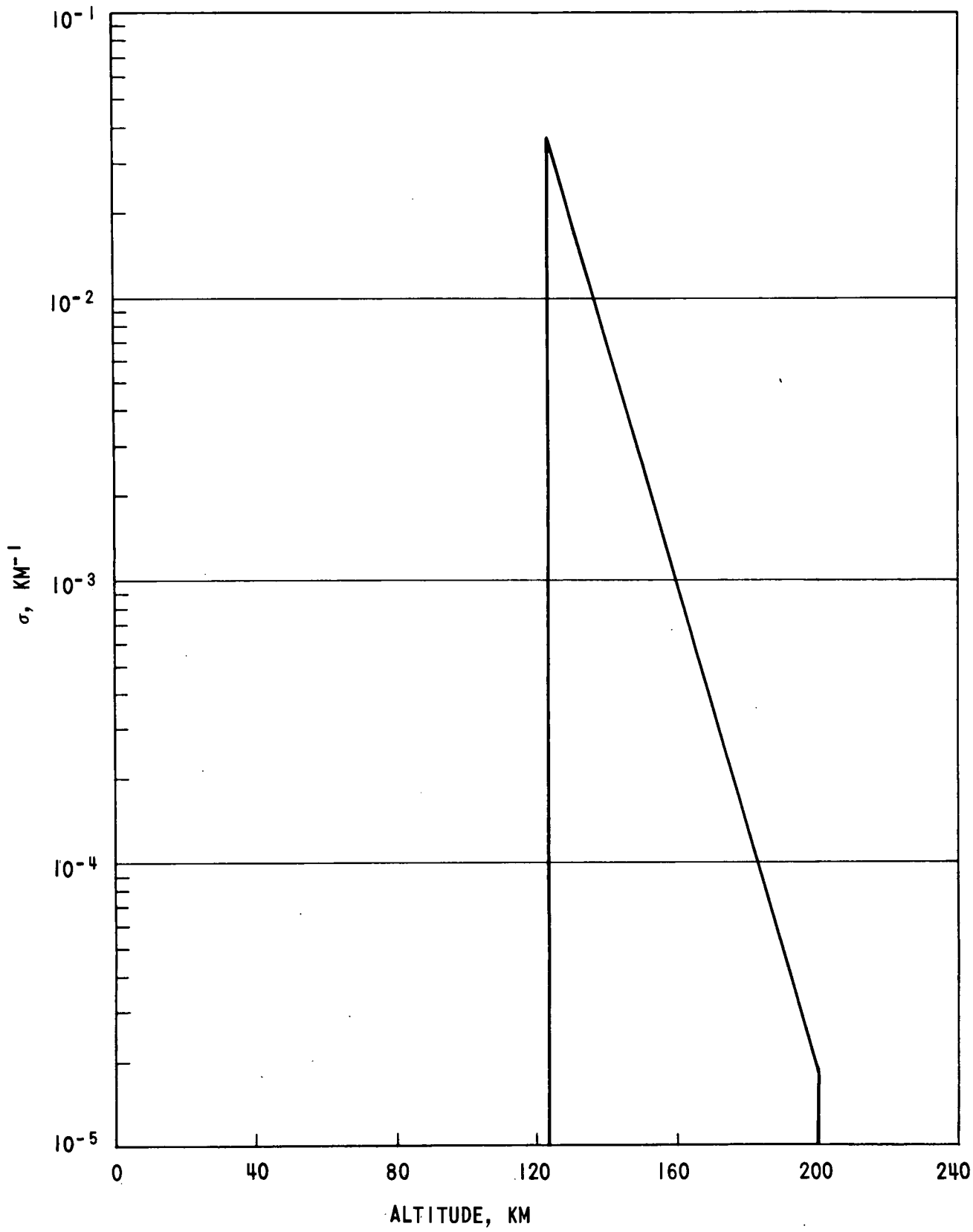


FIGURE 1 - VARIATION OF THE EXTINCTION COEFFICIENT WITH ALTITUDE FOR THE ADOPTED HAZE ATMOSPHERE

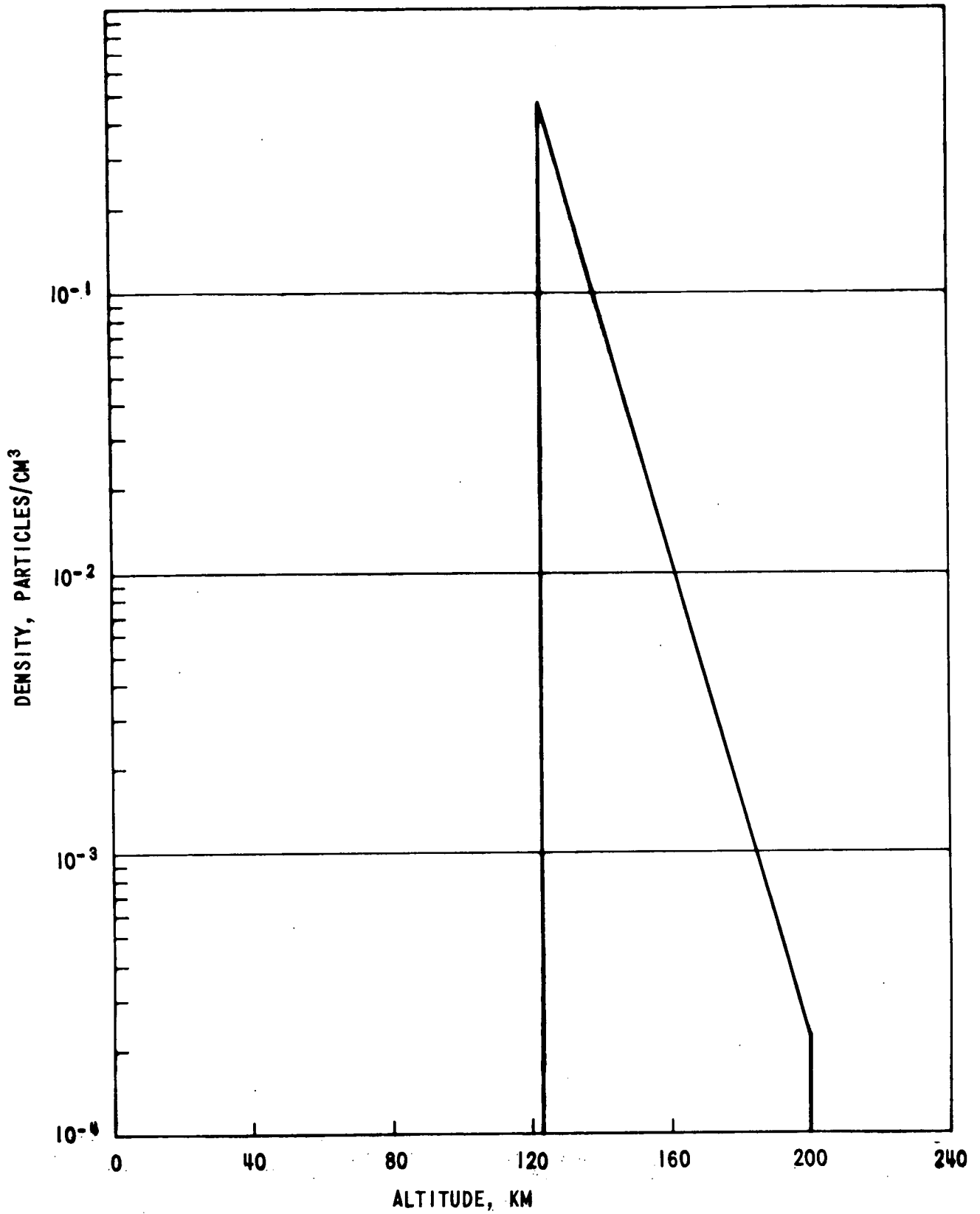


FIGURE 2 - DENSITY OF 10 MICRON PARTICLES REQUIRED TO PRODUCE THE EXTINCTION COEFFICIENT

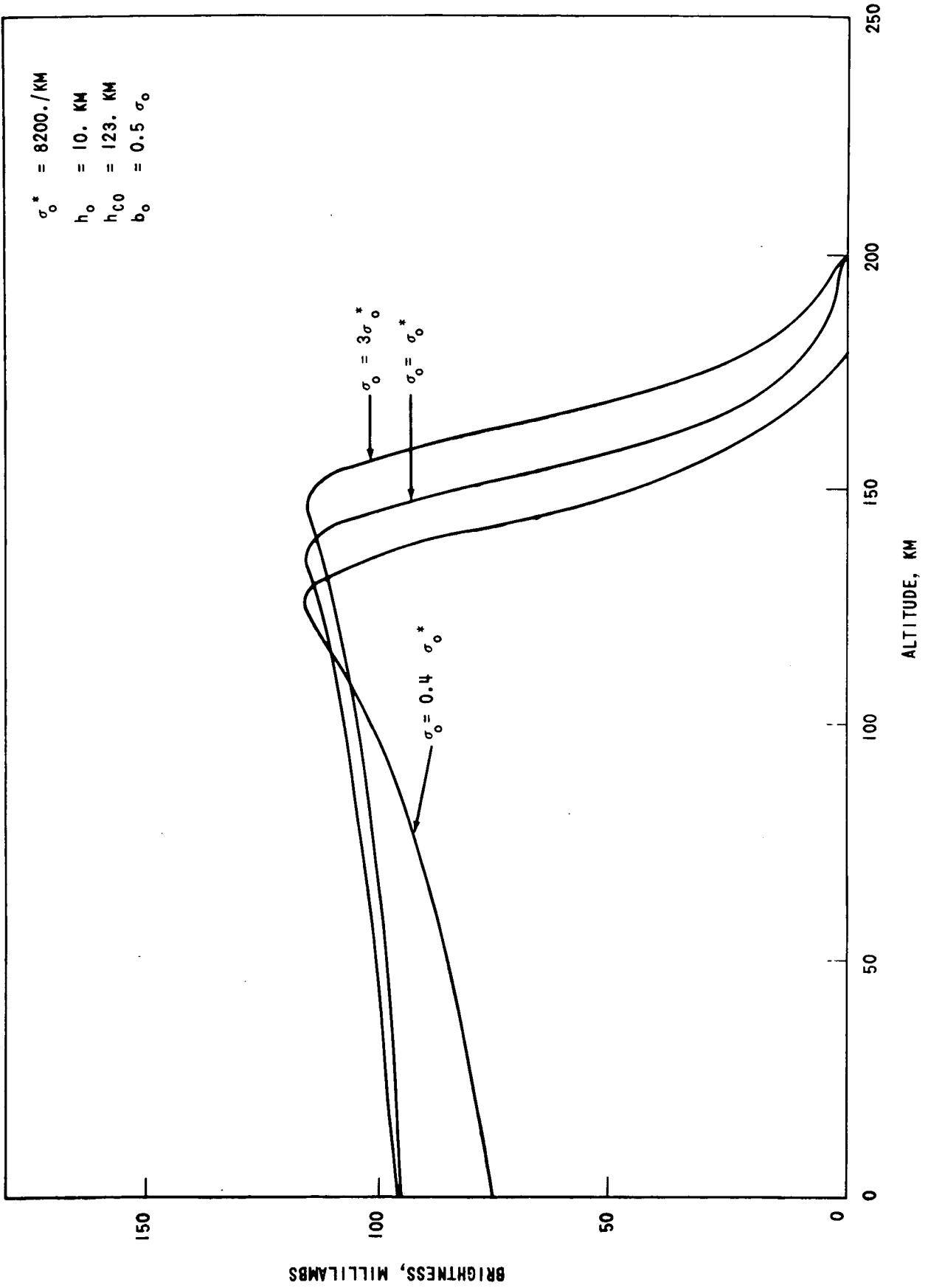


FIGURE 3 - VARIATION OF THE ATMOSPHERIC BRIGHTNESS PROFILE DUE TO CHANGES IN σ_0

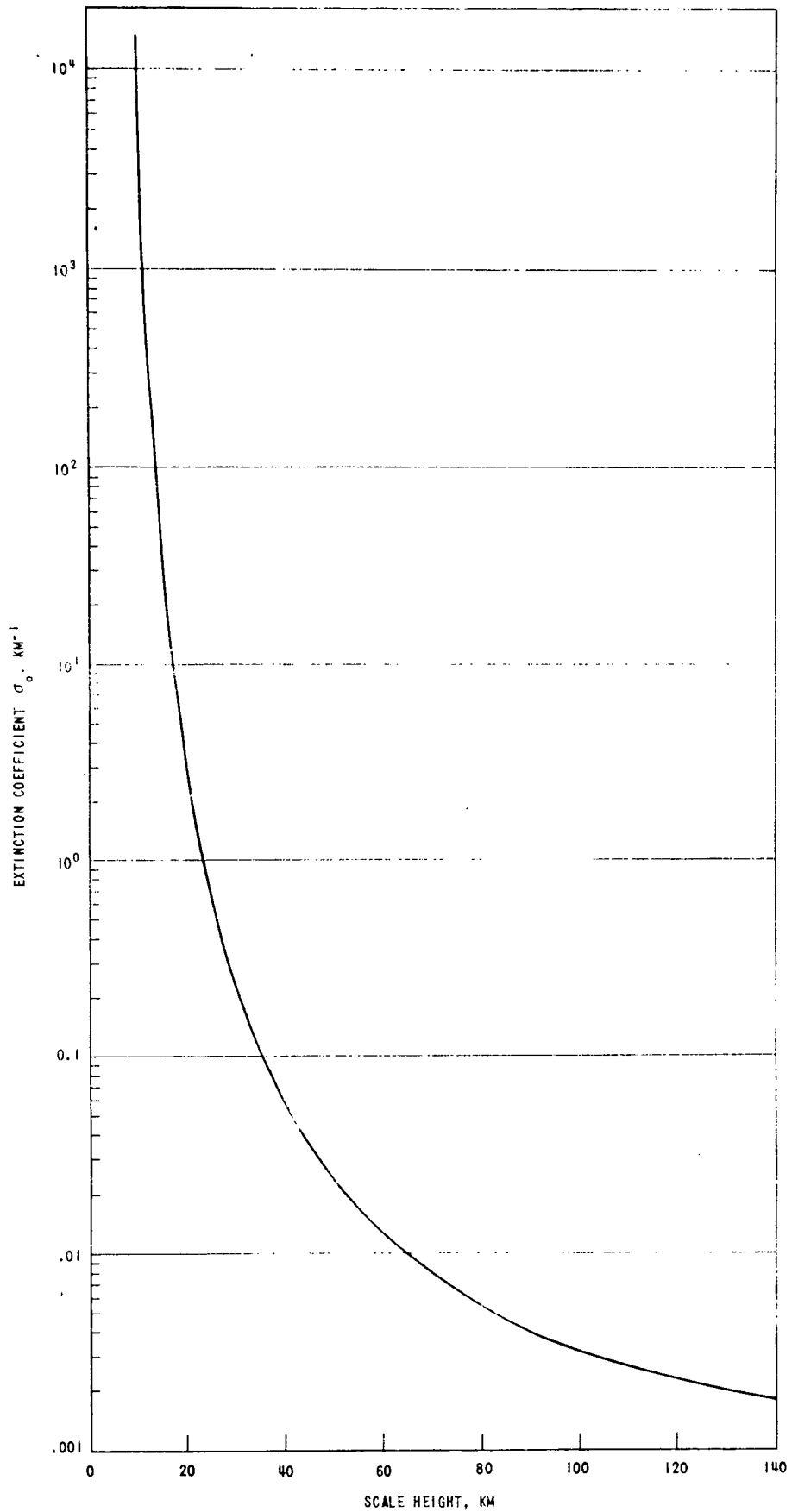


FIGURE 4 - MINIMUM VALUE OF σ_0 VERSUS SCALE HEIGHT

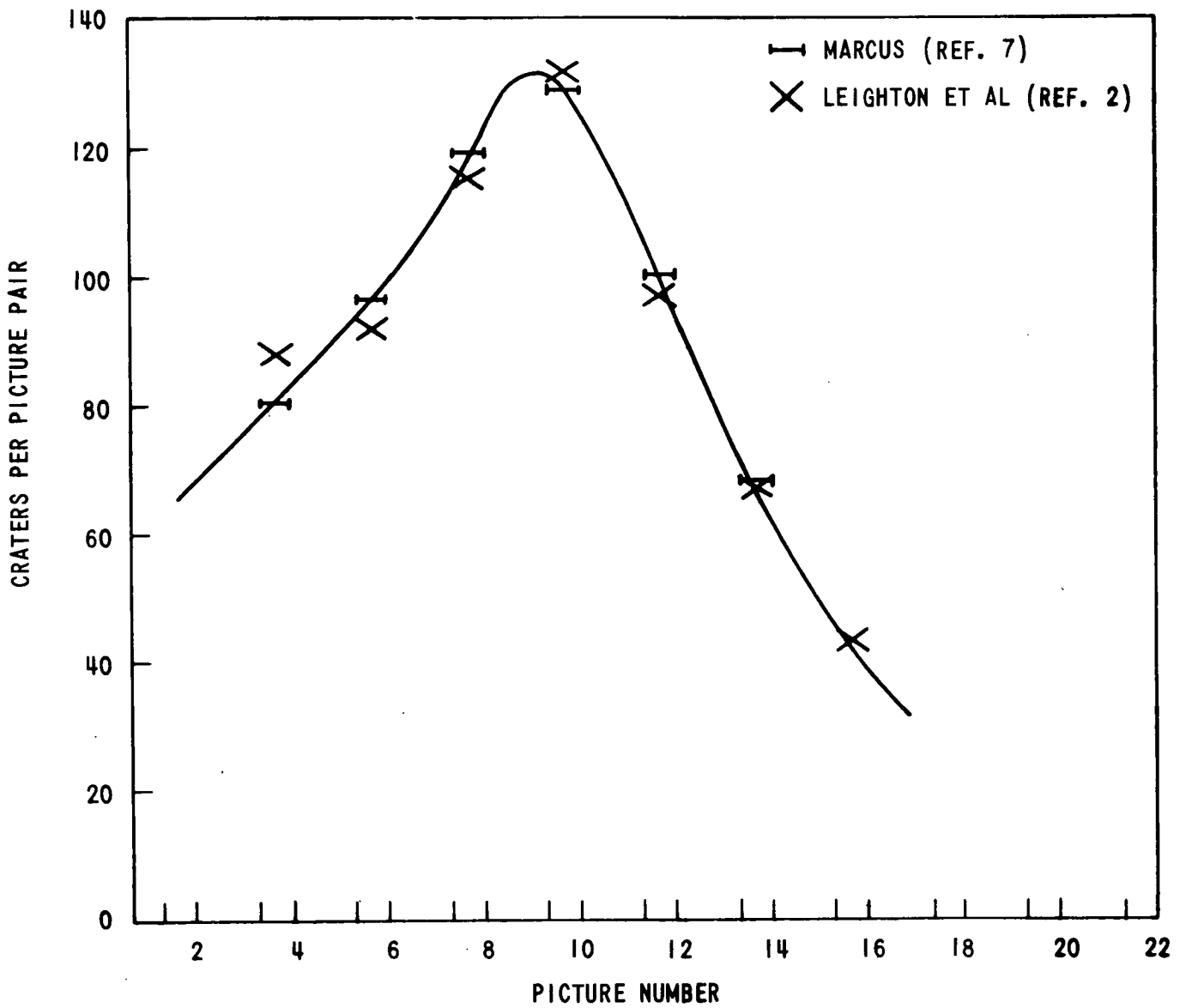


FIGURE 5 - NUMBER OF DETECTABLE CRATERS IN THE MARINER IV PICTURES

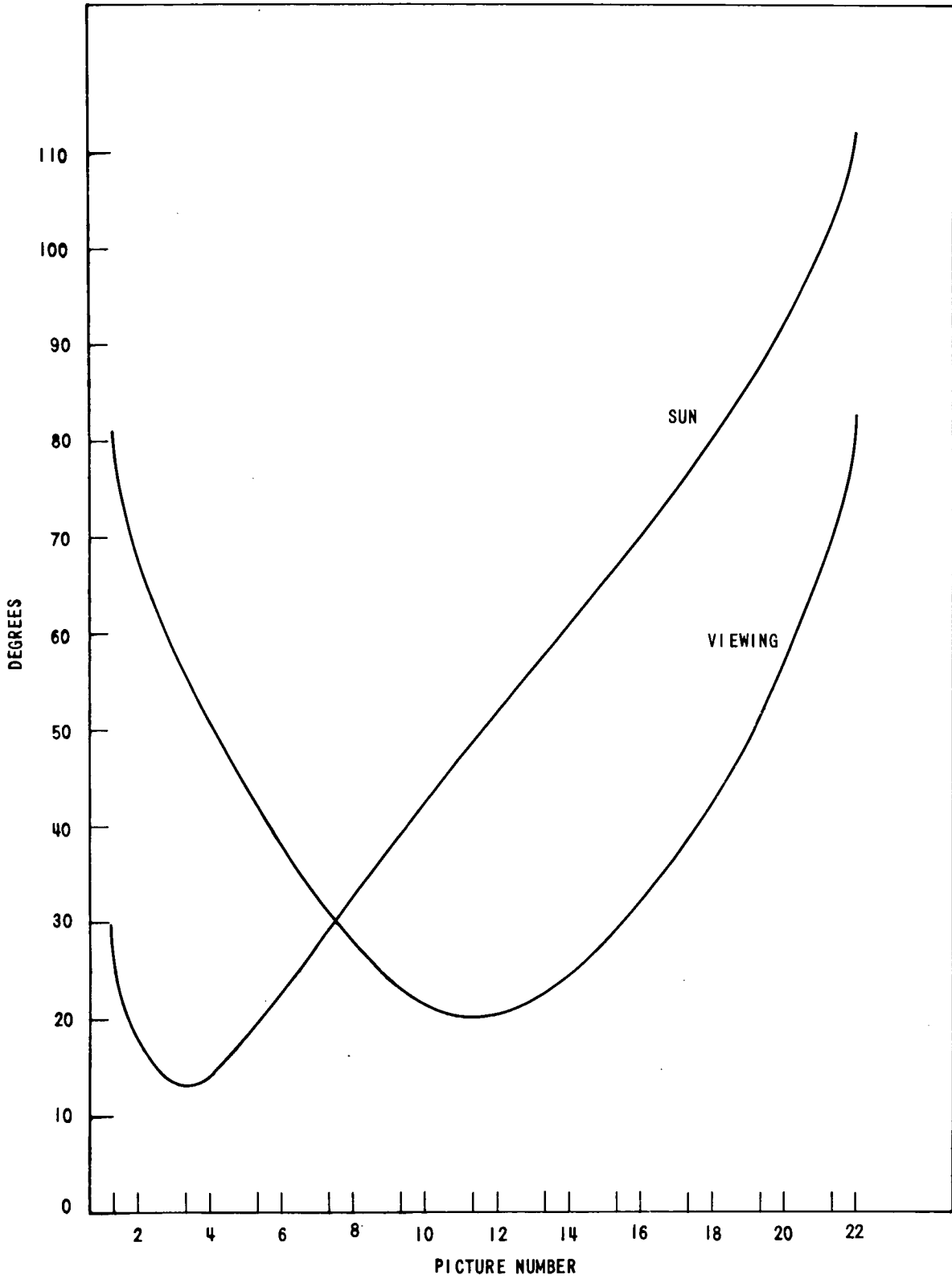


FIGURE 6 - PHOTOMETRIC GEOMETRY AT THE CENTER OF EACH OF THE MARINER IV PICTURES. THE ANGLES ARE MEASURED FROM THE LOCAL VERTICAL

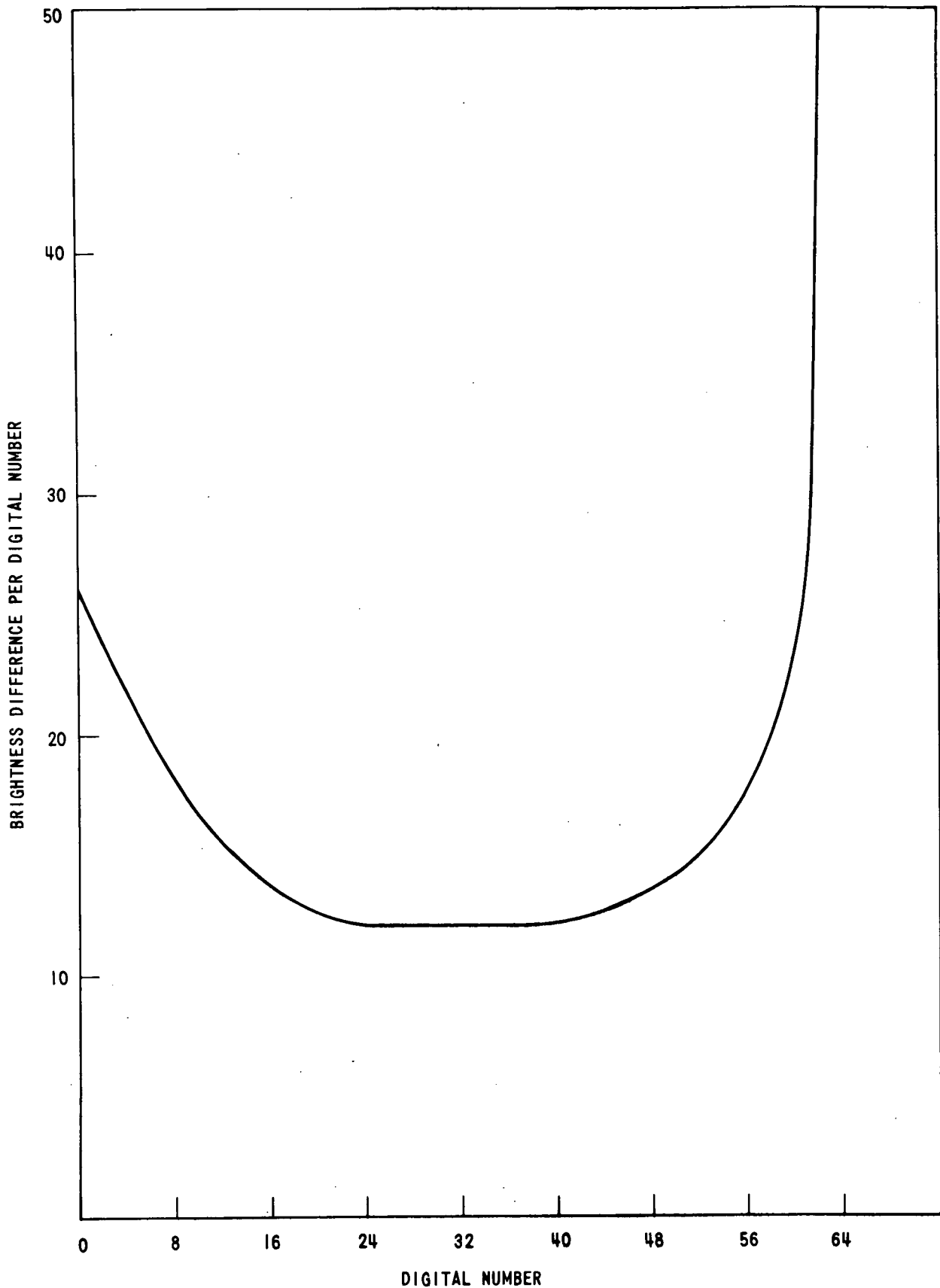


FIGURE 7 - BRIGHTNESS DIFFERENCES CORRESPONDING TO ONE DIGITAL NUMBER, AS A FUNCTION OF DIGITAL NUMBER. (REFERENCE 2)

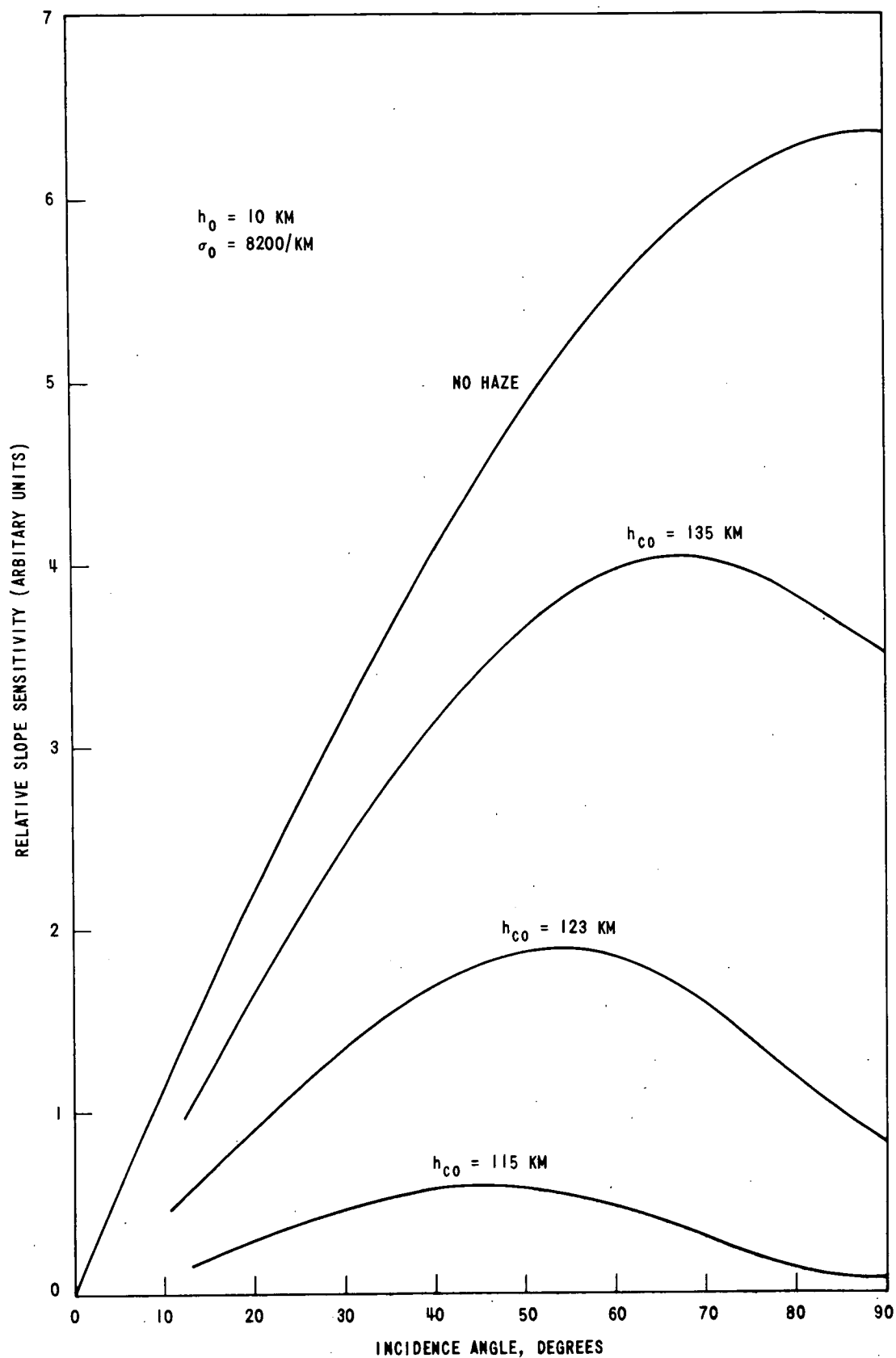


FIGURE 8 - SLOPE SENSITIVITY FOR VARIOUS VALUES OF THE LOW ALTITUDE CUTOFF. FOR EACH INCIDENCE ANGLE, THE VIEWING ANGLE WAS TAKEN TO BE THAT APPROPRIATE TO THE MARINER IV TRAJECTORY.

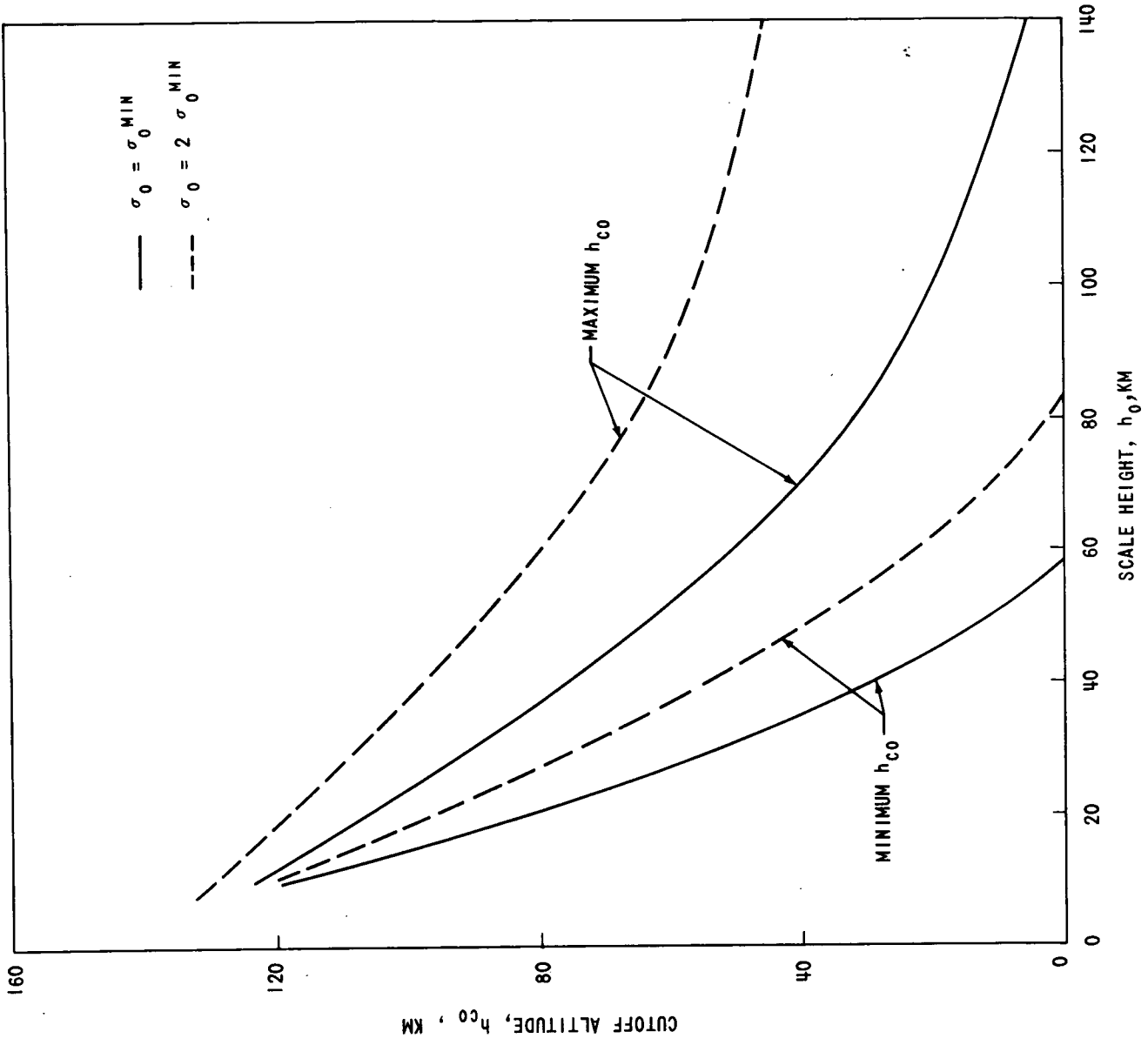


FIGURE 9 - MINIMUM AND MAXIMUM VALUES OF THE LOW ALTITUDE CUTOFF GIVEN AS A FUNCTION OF THE SCALE HEIGHT. FOR EACH SCALE HEIGHT, $\sigma_0 \text{ MIN}$ WAS OBTAINED FROM FIGURE 4.

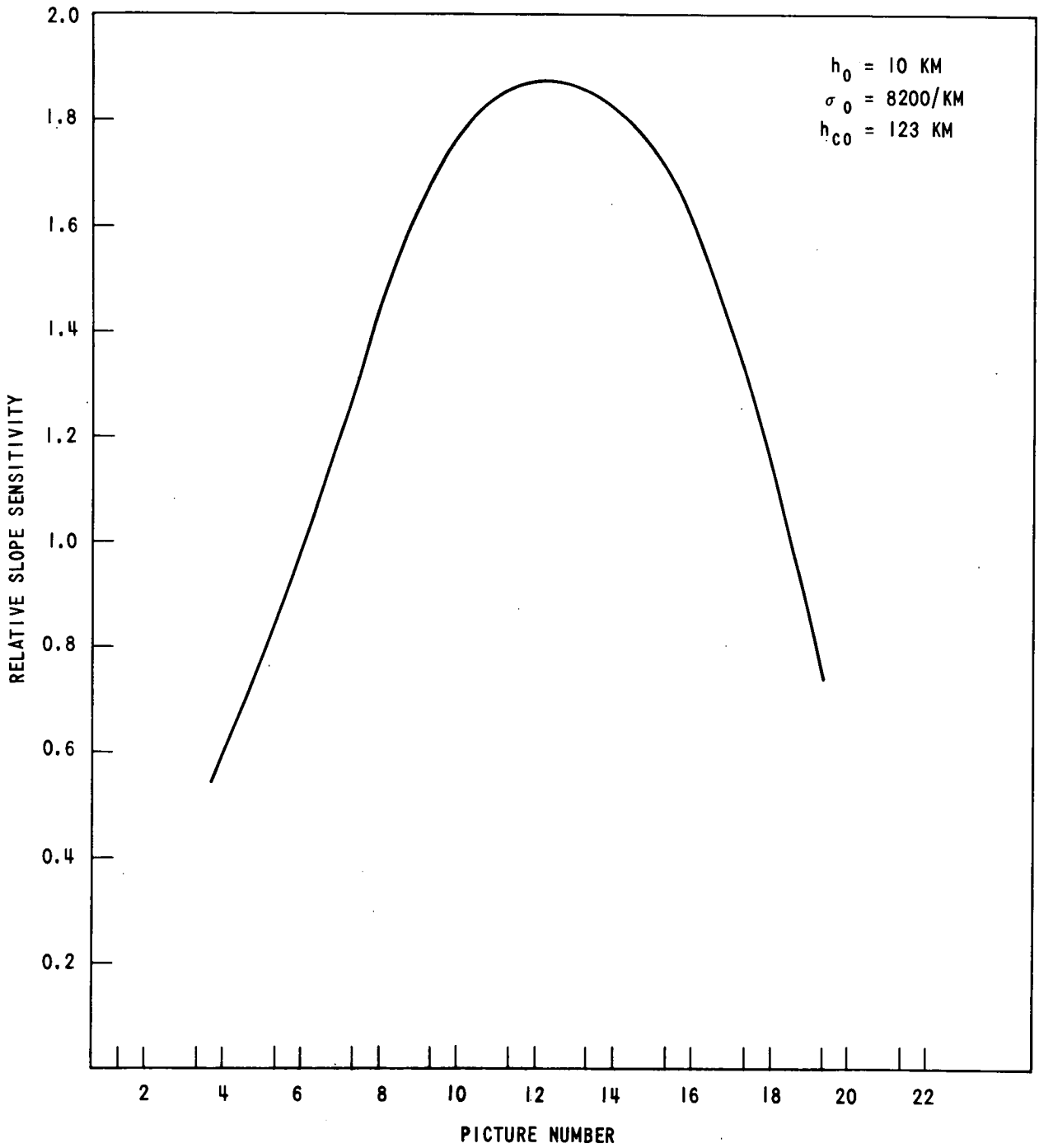


FIGURE 10 - CALCULATED SLOPE SENSITIVITY IN THE PRESENCE OF HAZE.

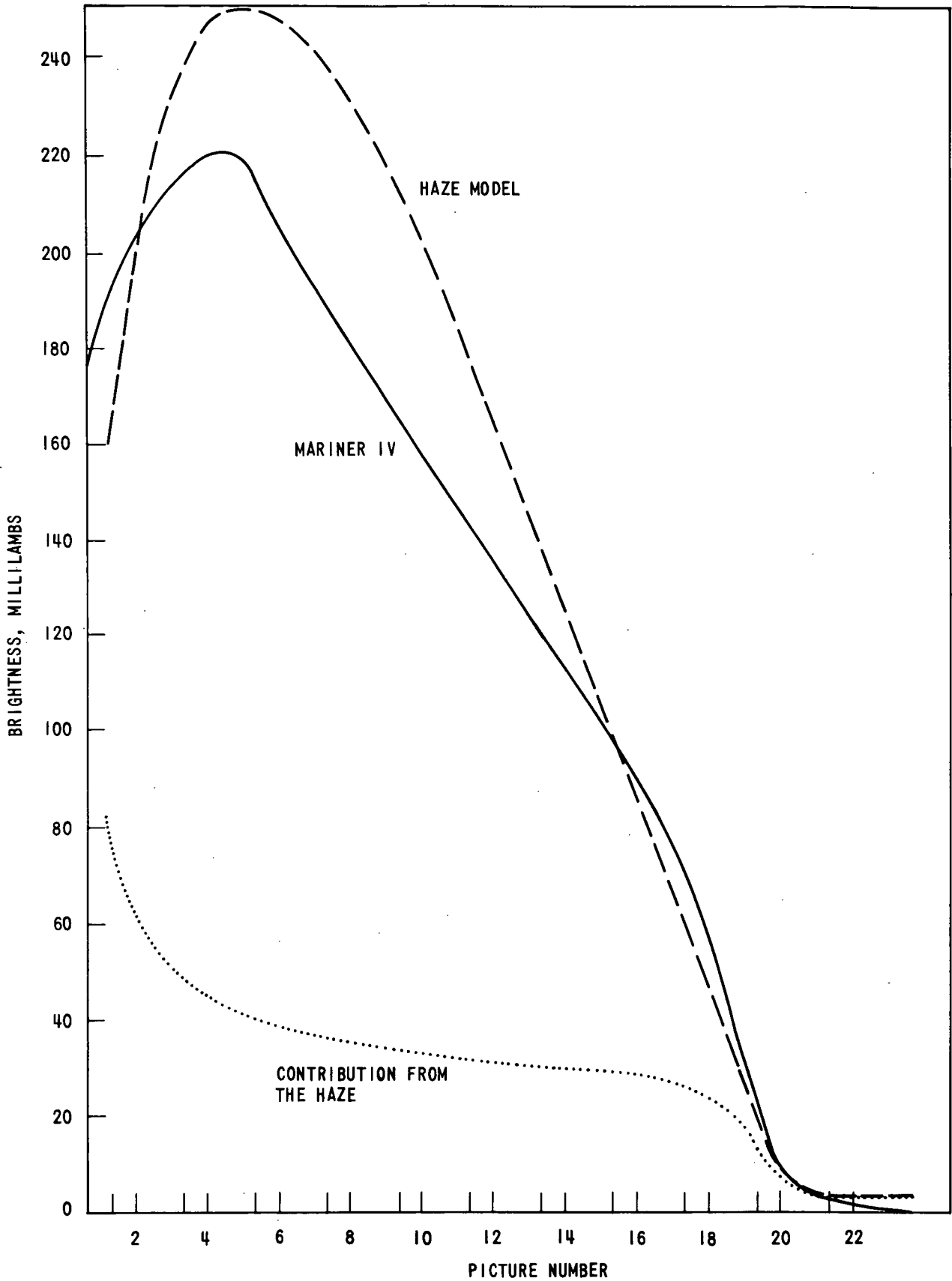


FIGURE 11 - CALCULATED AND MEASURED BRIGHTNESS FOR THE MARINER IV PICTURES. THE CALCULATED BRIGHTNESSES WERE OBTAINED FOR THE ADOPTED SET OF PARAMETERS GIVEN IN TABLE I.

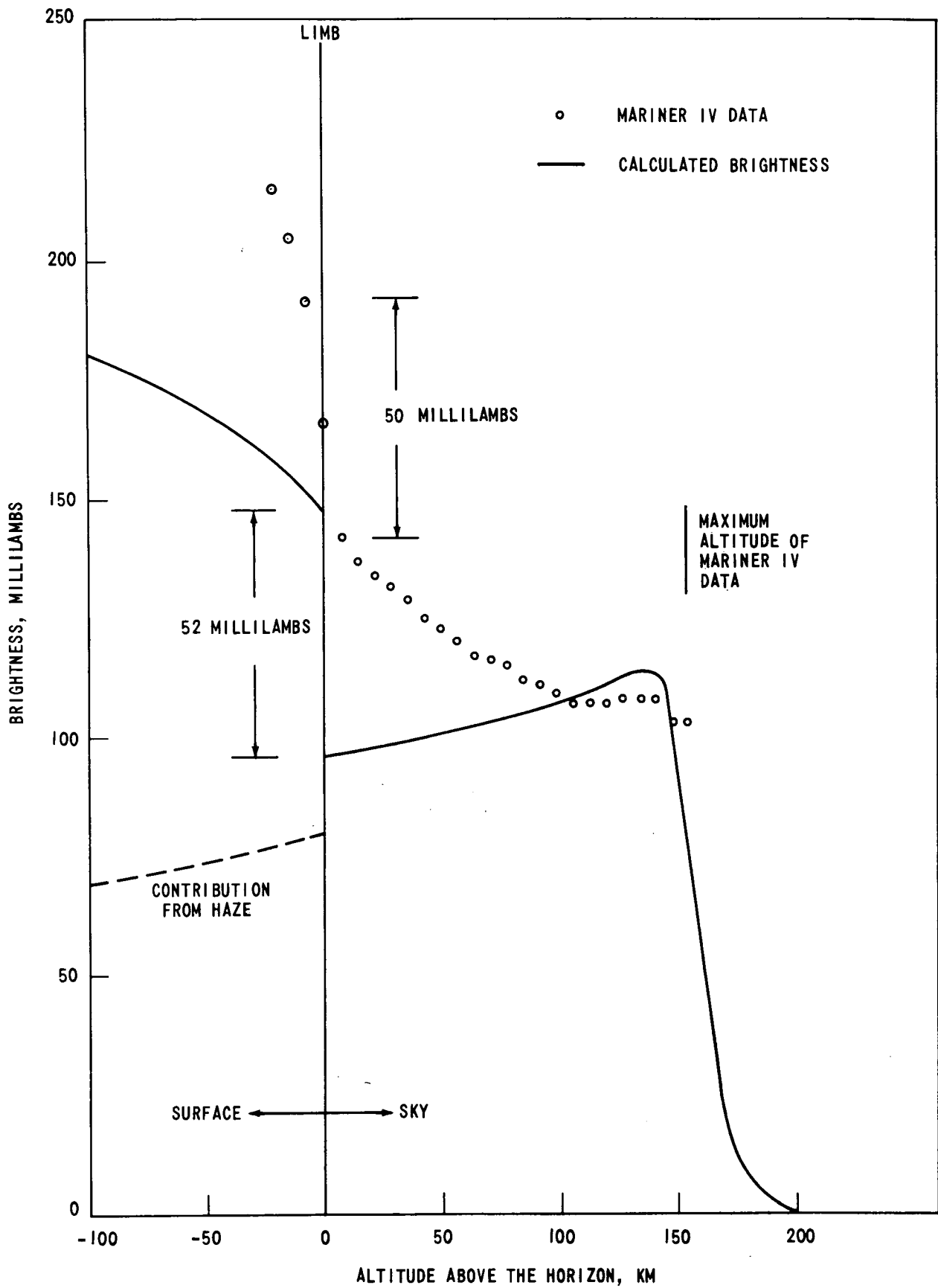


FIGURE 12 - BRIGHTNESS DISCONTINUITY OF THE LIMB OF THE PLANET.

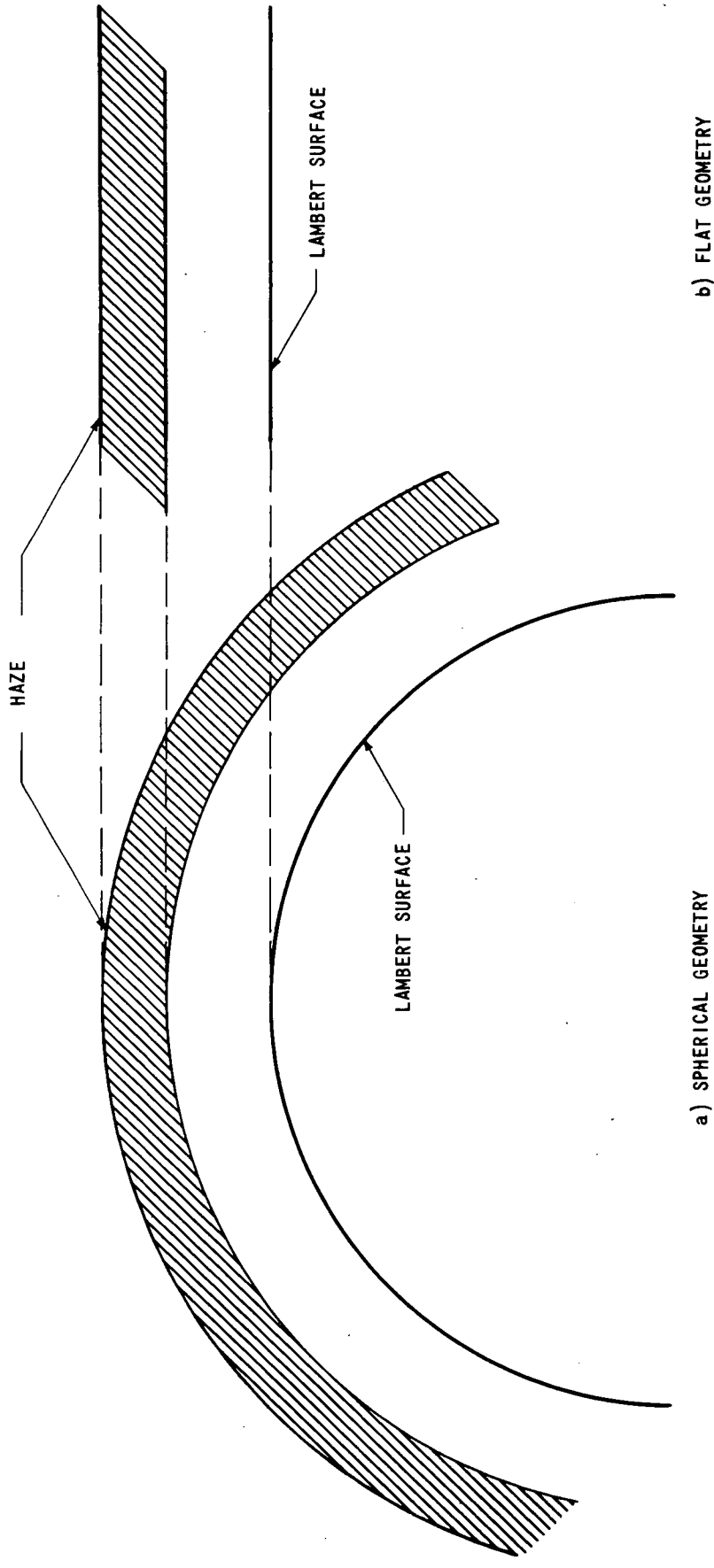


FIGURE 13 - COMPARISON OF THE GEOMETRIES USED FOR THE FLAT AND THE SPHERICAL BRIGHTNESS CALCULATIONS.

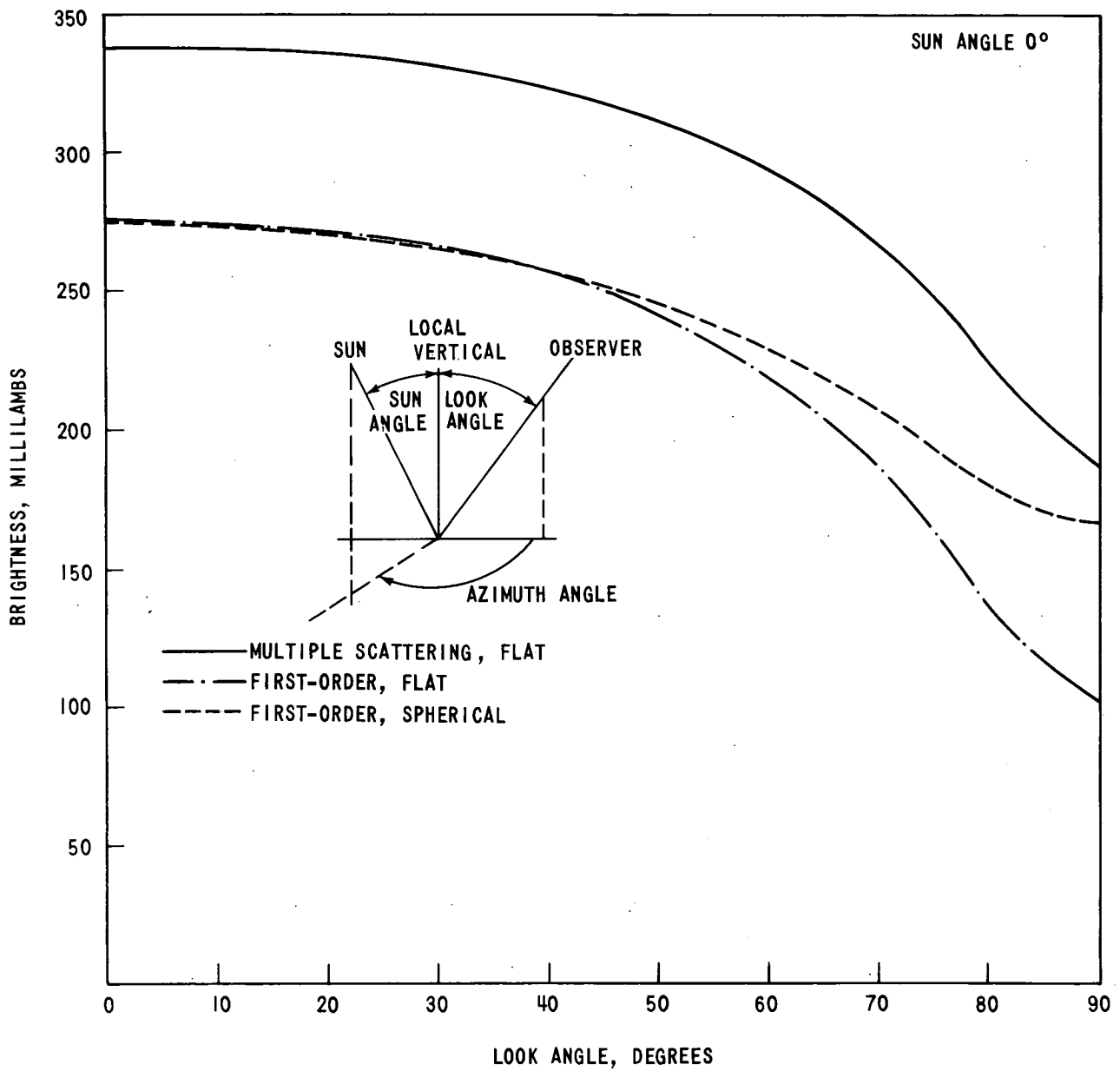


FIGURE 14 - THE BRIGHTNESS AS A FUNCTION OF LOOK ANGLE FOR A FIXED SUN ANGLE OF 0°

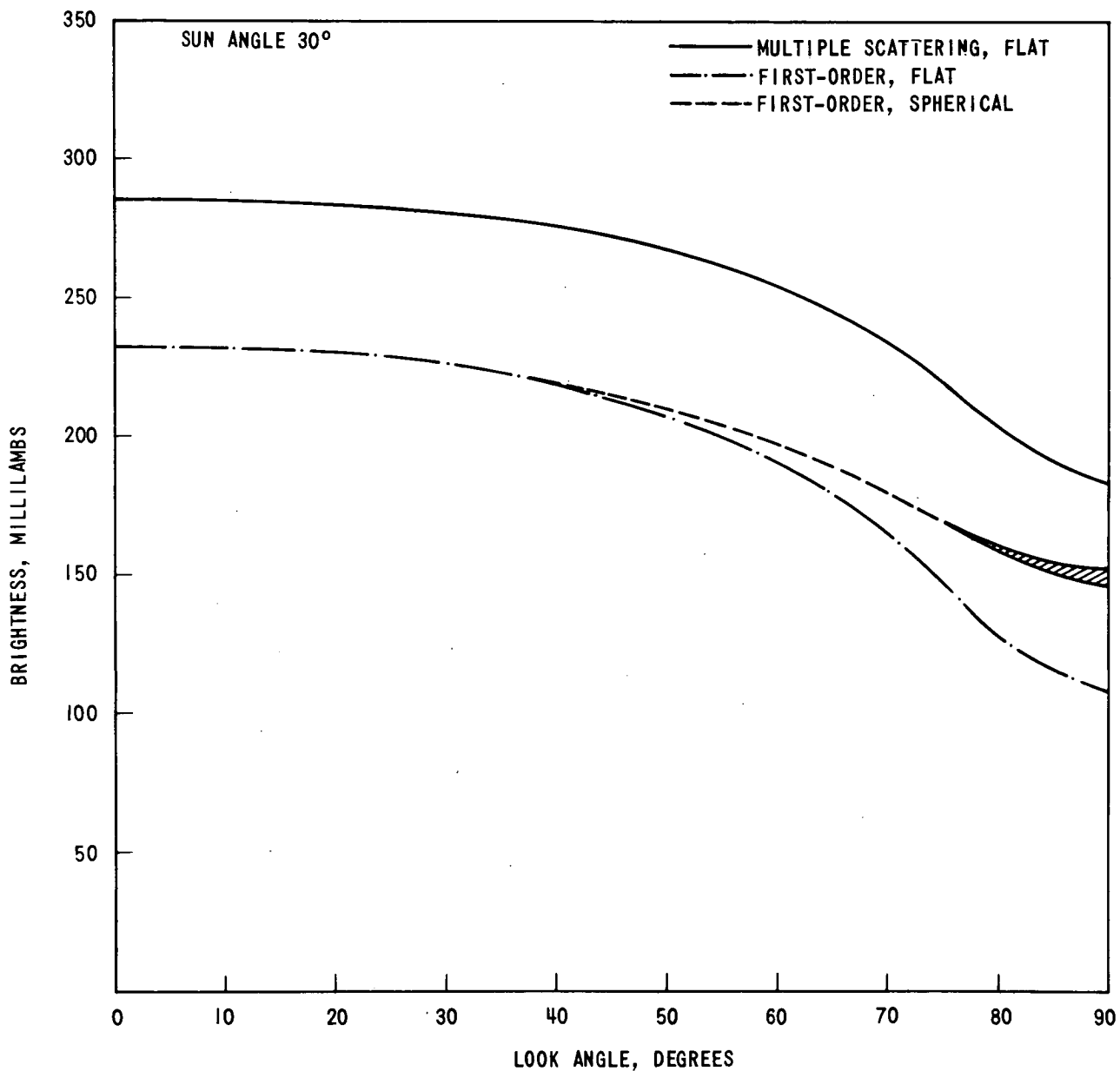


FIGURE 15 - THE BRIGHTNESS AS A FUNCTION OF LOOK ANGLE FOR A FIXED SUN ANGLE OF 30°. THE CROSS-HATCHED AREA REPRESENTS THE RANGE OF VALUES ARISING FROM THE AZIMUTHAL DEPENDENCE IN THE FIRST ORDER SPHERICAL CALCULATIONS.

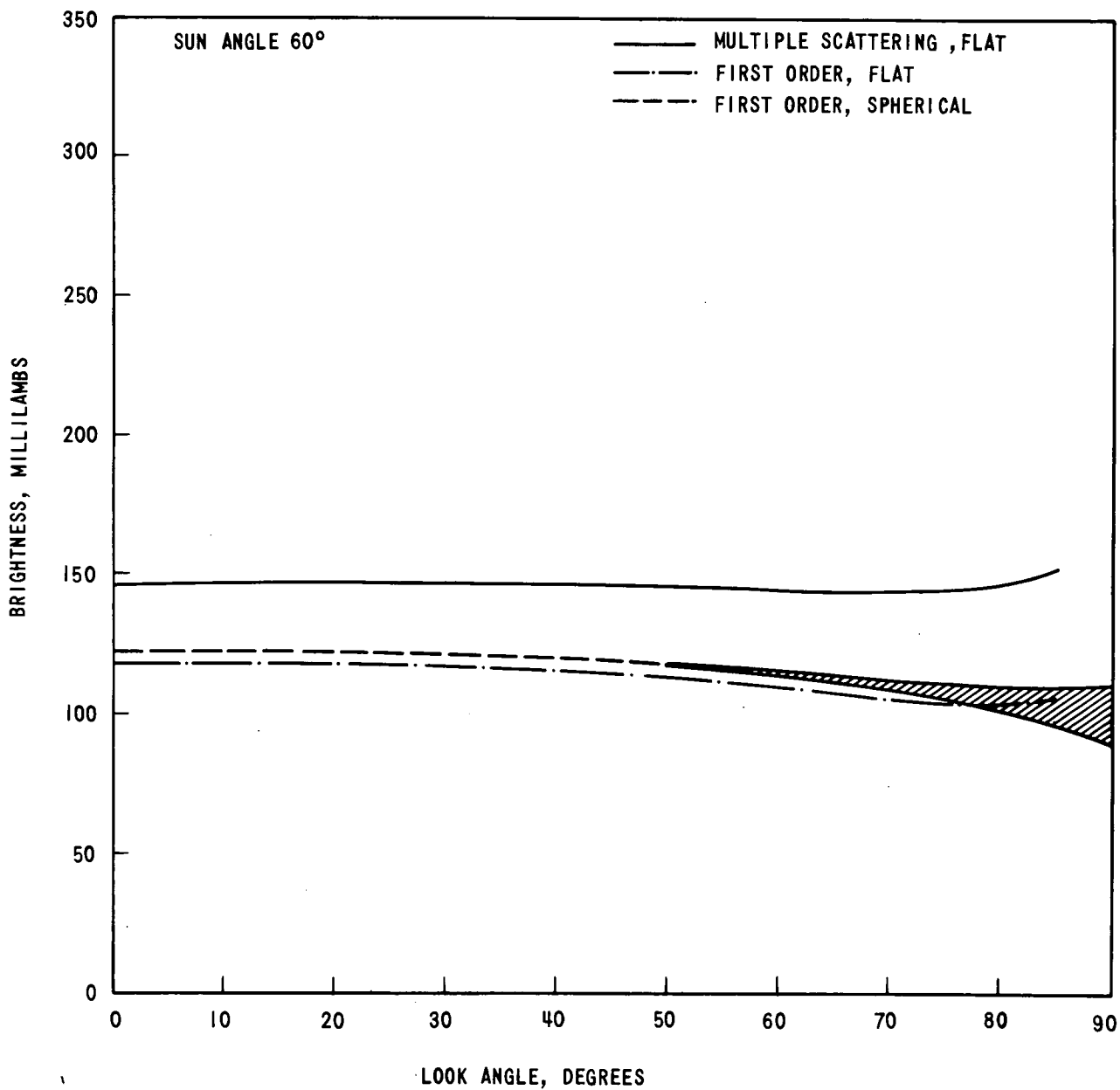


FIGURE 16 - THE BRIGHTNESS AS A FUNCTION OF LOOK ANGLE FOR A FIXED SUN ANGLE OF 60°. THE CROSS-HATCHED AREA REPRESENTS THE RANGE OF VALUES ARISING FROM THE AZIMUTHAL DEPENDENCE IN THE FIRST ORDER SPHERICAL CALCULATIONS.

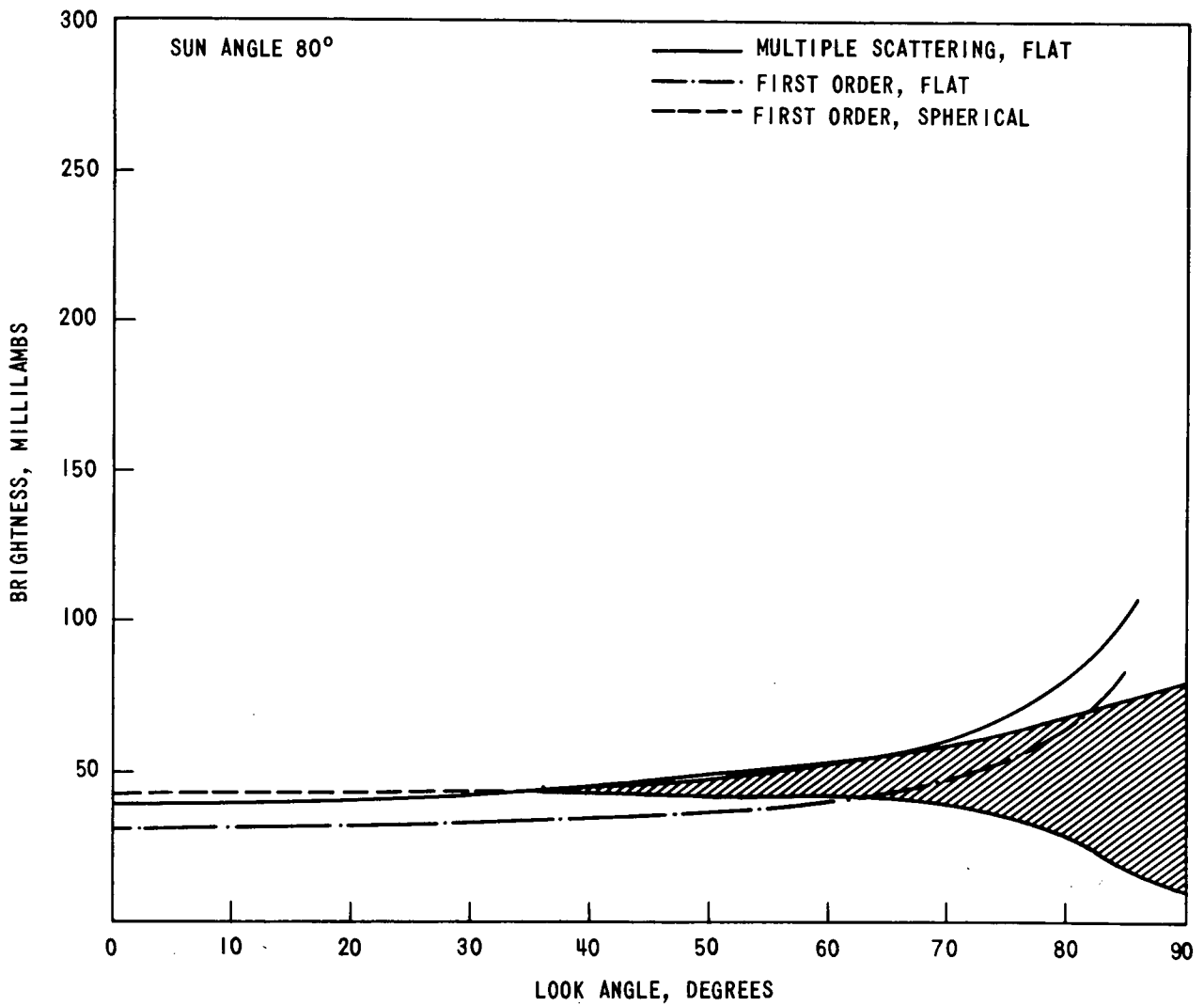


FIGURE 17 - THE BRIGHTNESS AS A FUNCTION OF LOOK ANGLE FOR A FIXED SUN ANGLE OF 80°. THE CROSS-HATCHED AREA REPRESENTS THE RANGE OF VALUES ARISING FROM THE AZIMUTHAL DEPENDENCE IN THE FIRST ORDER SPHERICAL CALCULATIONS.

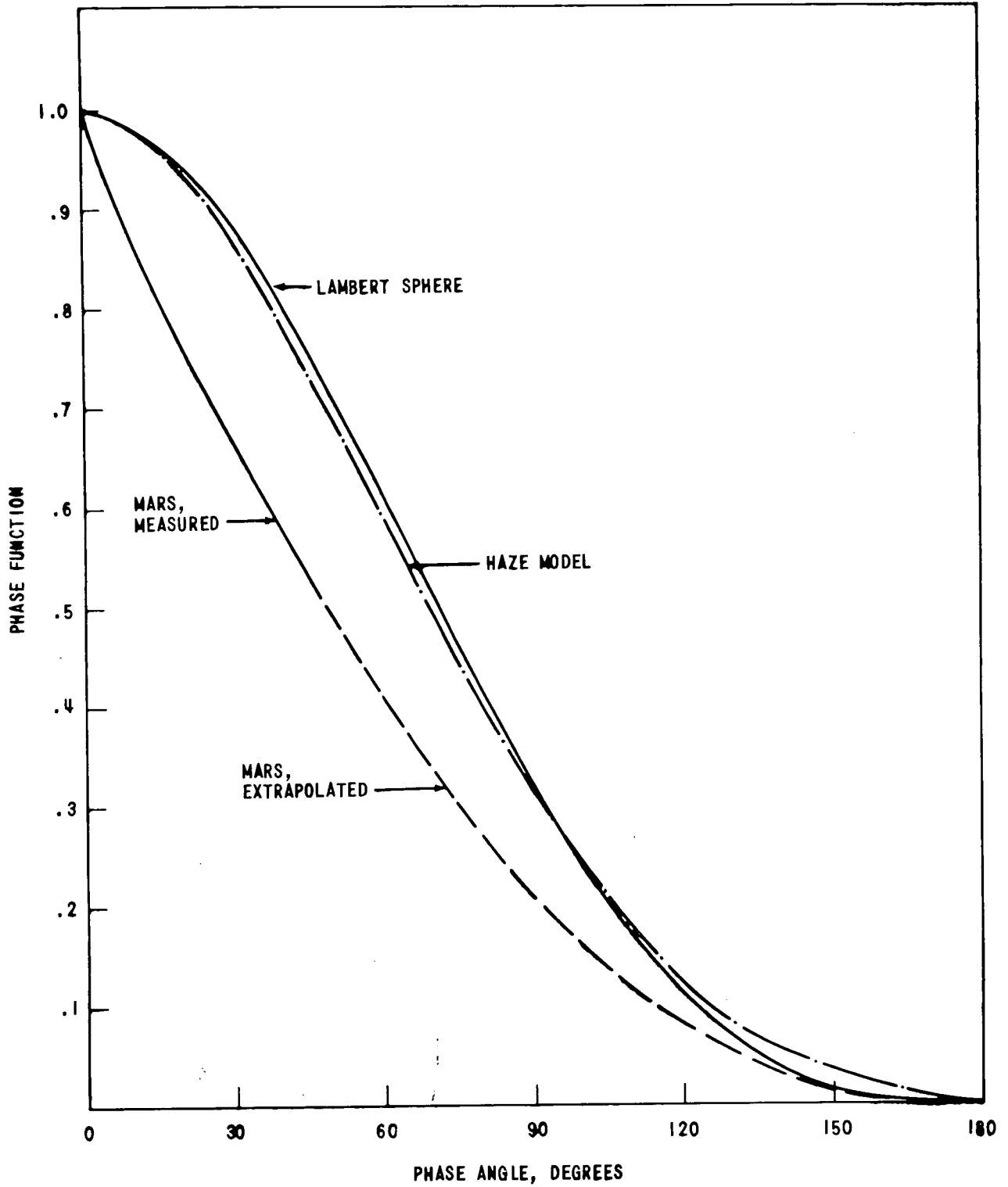


FIGURE 18 - CALCULATED PHASE FUNCTION FOR MARS COMPARED TO THE OBSERVED DATA. THE PHASE FUNCTION FOR A SPHERE WITH A LAMBERT SURFACE IS ALSO SHOWN.

PHASE ANGLE 0°

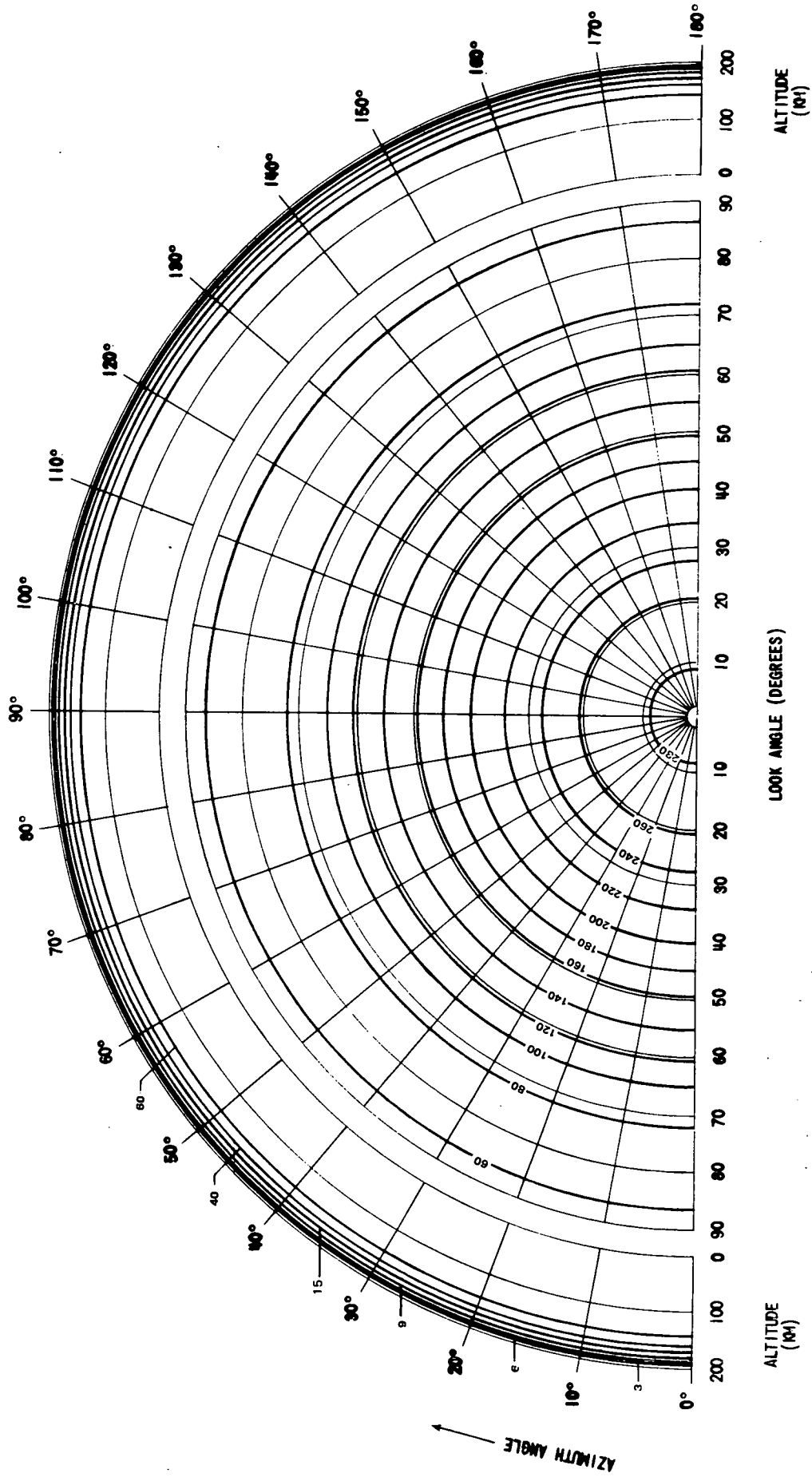


FIGURE 19 - ISO-BRIGHTNESS CONTOURS. THE UNITS OF BRIGHTNESS ARE MILLILAMBS

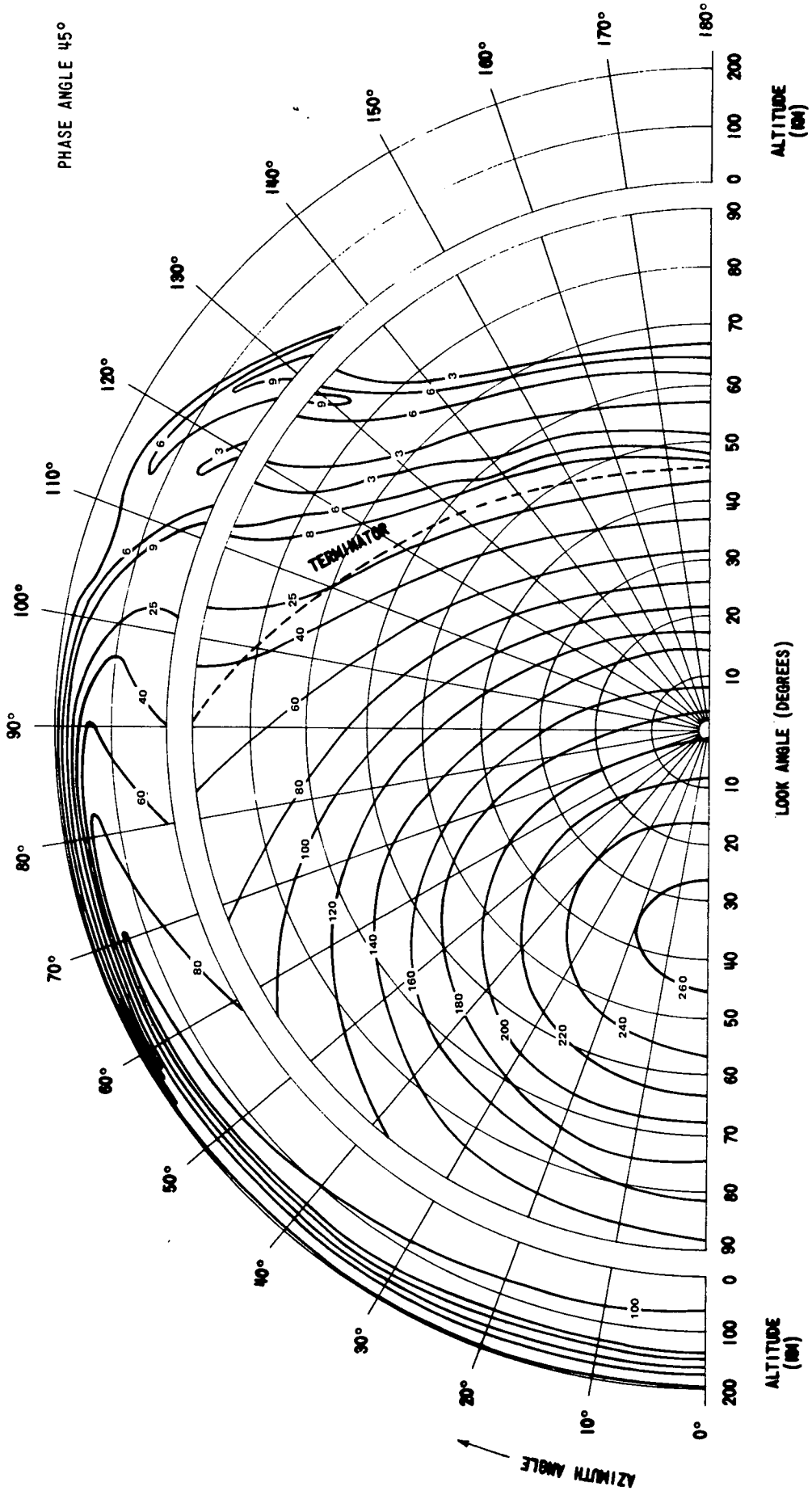


FIGURE 20 - 150-BRIGHTNESS CONTOURS. THE UNITS OF BRIGHTNESS ARE MILLILAMBS

PHASE ANGLE 90°

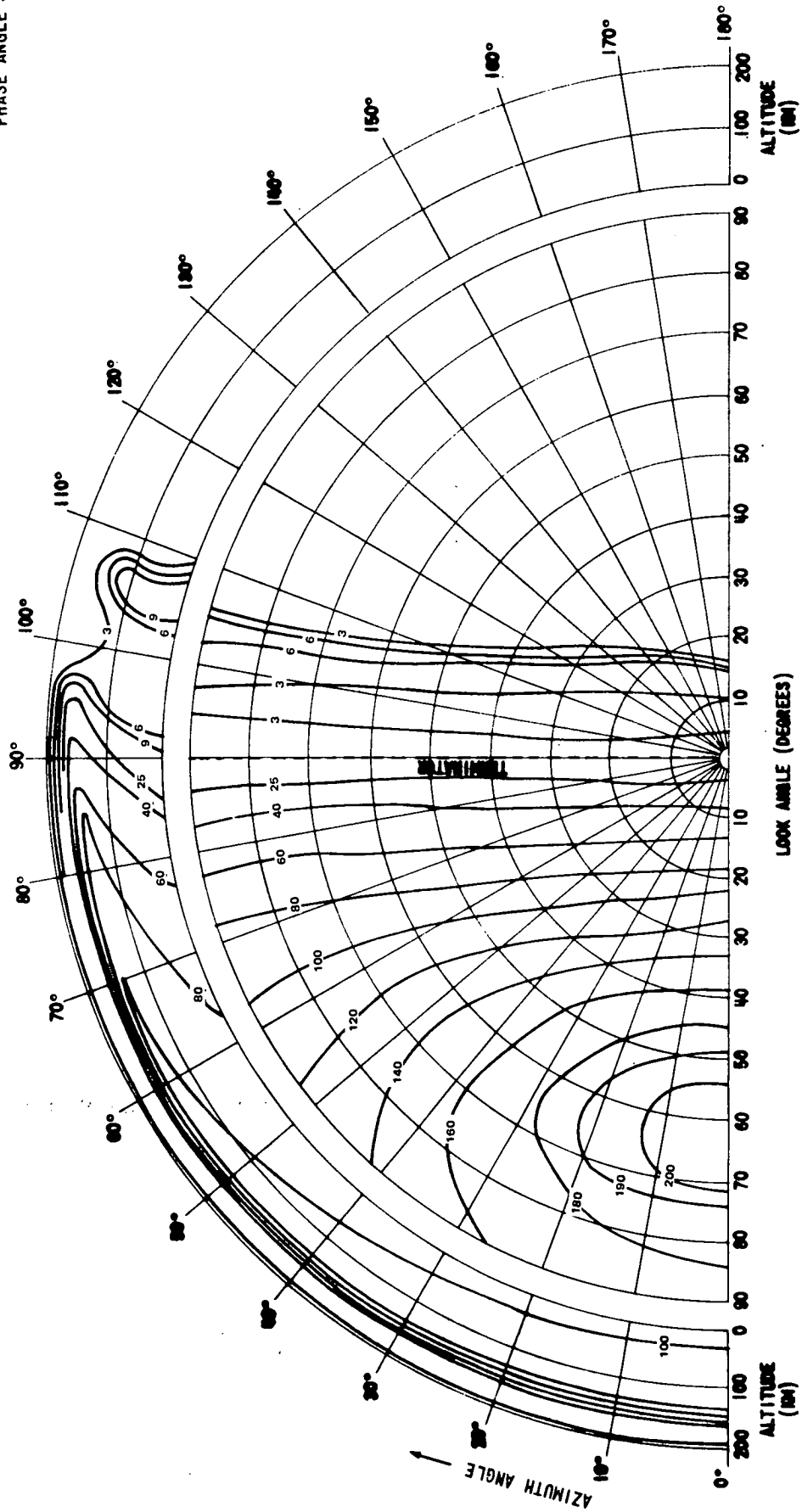


FIGURE 21 - 150-BRIGHTNESS CONTOURS. THE UNITS OF BRIGHTNESS ARE MILLILAMBS

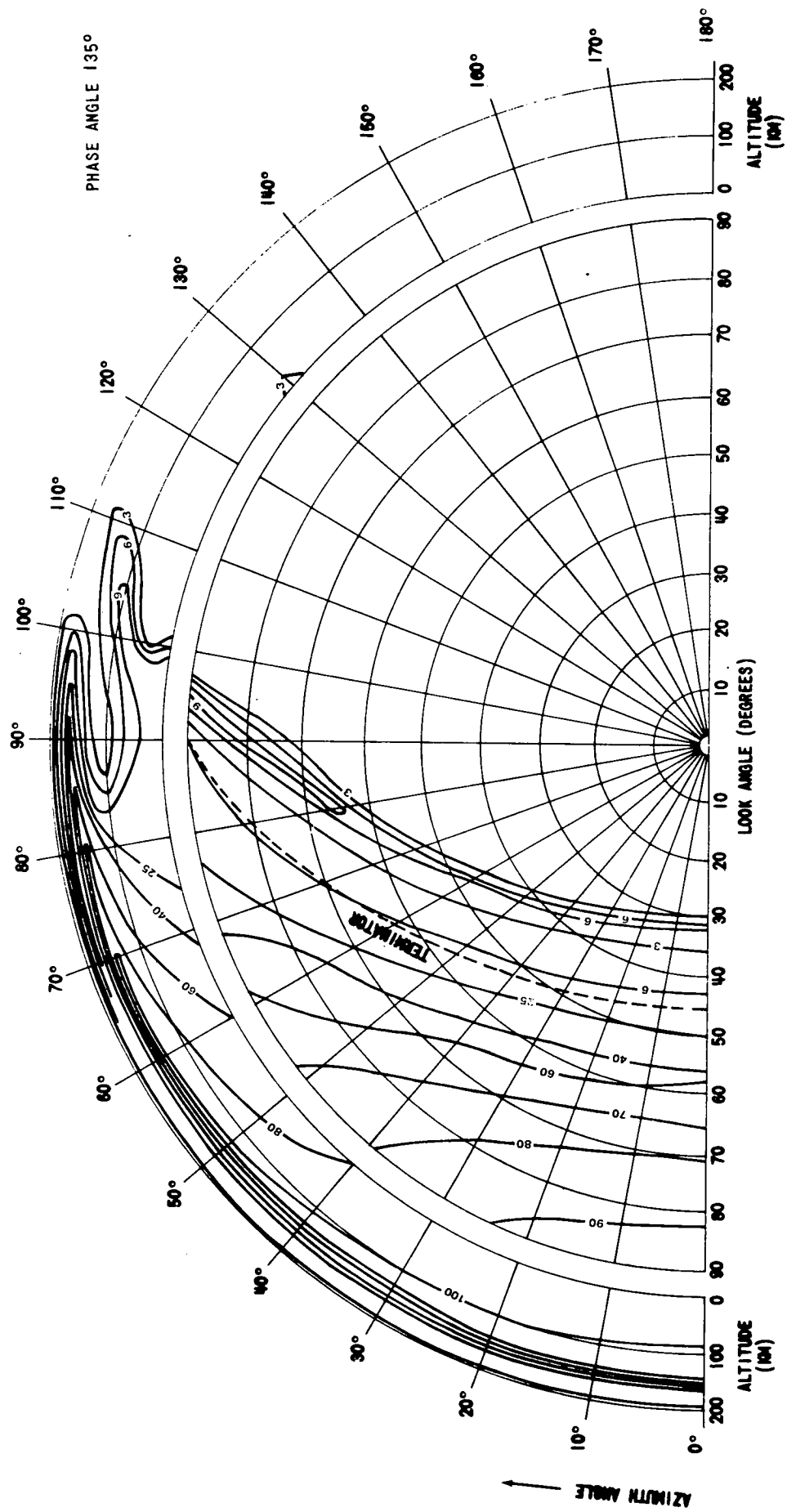
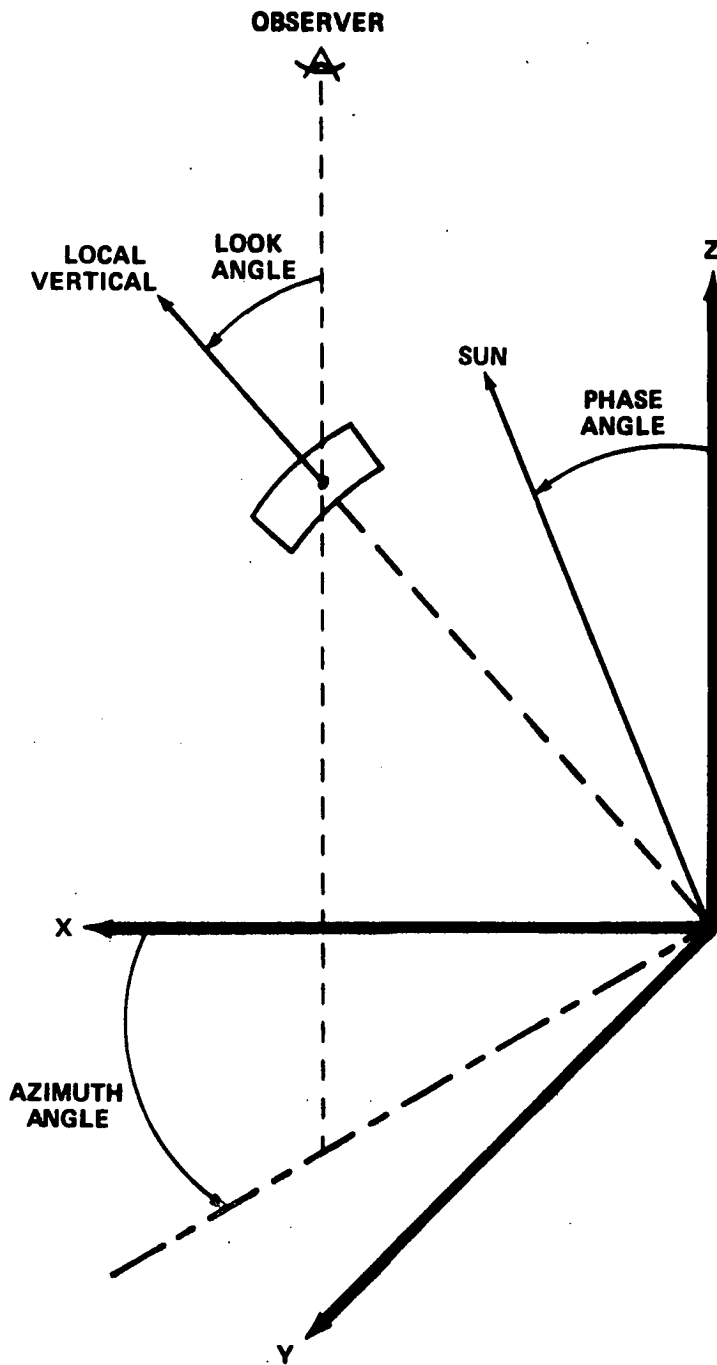


FIGURE 22 - 150-BRIGHTNESS CONTOURS. THE UNITS OF BRIGHTNESS ARE MILLILAMBS



**FIGURE 23 - ILLUSTRATION OF THE ANGLES USED IN THE BRIGHTNESS PLOTS.
THE SUN LIES IN THE X-Z PLANE.**

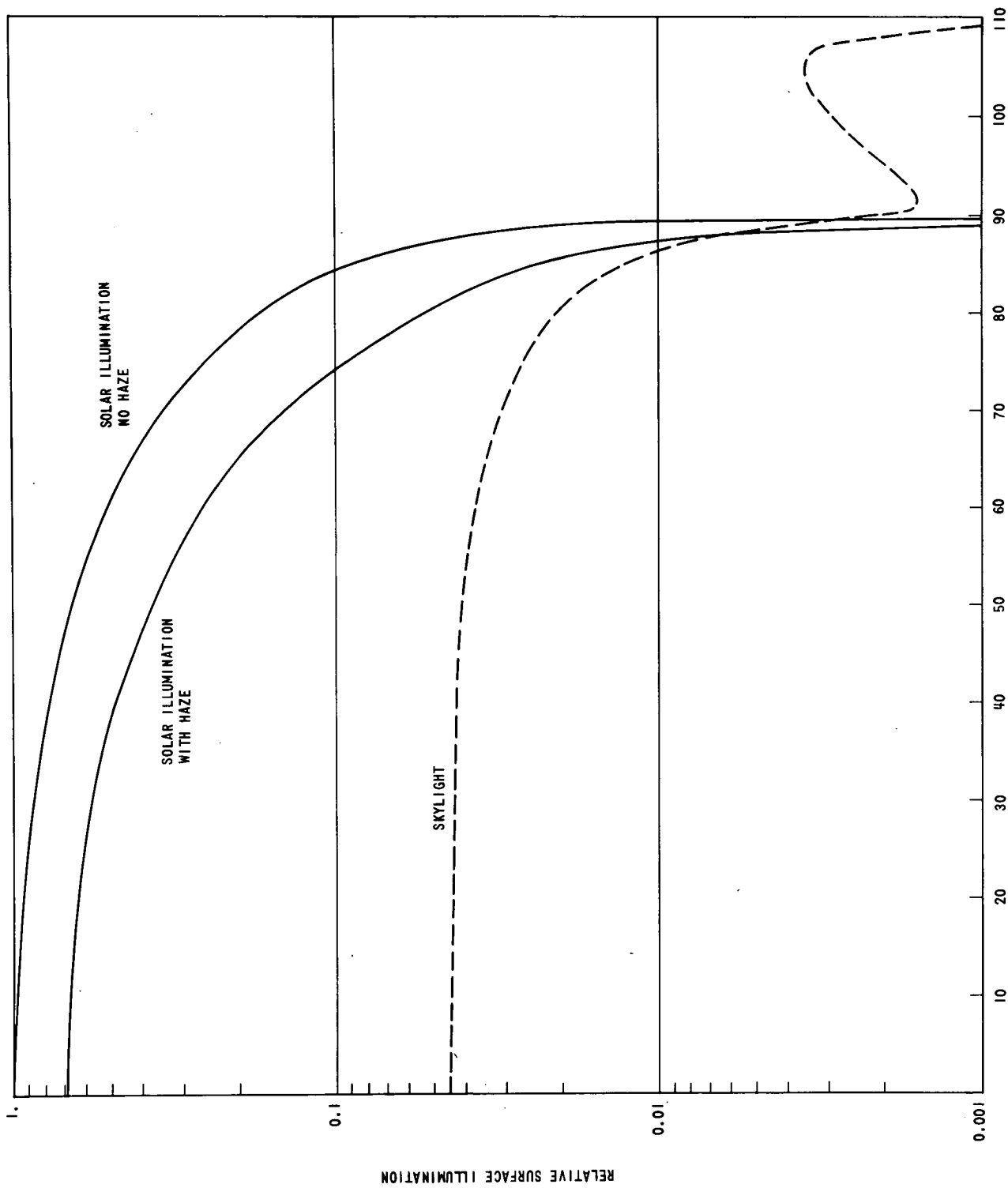


FIGURE 24 - ILLUMINATION OF THE SURFACE. THE CURVES ARE NORMALIZED TO THE FLUX IN THE INCIDENT RADIATION.

APPENDIX A

FIRST-ORDER THEORY

In this section, the differential equation governing the apparent brightness seen by an observer will be derived. We will be concerned with the line of sight of an observer who may be above the haze, somewhere in the haze, or on the surface of the planet. The line of sight may extend through the atmosphere or intersect the surface.

The distance along the line of sight, χ , increases as one moves toward the observer. To each point χ is associated a vector $\vec{r}(\chi)$ which locates the point relative to the center of the planet. The atmospheric properties and the local brightness are functions of \vec{r} . In addition, we establish a local coordinate system, centered at $\vec{r}(\chi)$ and oriented such that the z axis lies along the line of sight, the x axis is in the plane of the line of sight and the vector \vec{r} , and the y axis completes a right handed orthogonal coordinate system. This is illustrated in Figure A-1.

Consider a small volume element $dx \cdot dy \cdot dz$ located at χ . There are two sources of light incident on the volume element; these are the direct solar radiation, attenuated in passing through the atmosphere, and the light which has been scattered from other points within the atmosphere.

The differential equation describes the change in the apparent brightness in the direction of the observer as one moves from χ to $\chi + d\chi$. We have

$$\frac{d\omega}{d\chi} = -\sigma(\vec{r})\omega(\vec{r}, 0, 0) + \frac{b(\vec{r})}{4\pi} \cdot \pi F e^{-\tau_s} + \int \beta(\vec{r}, \theta) \omega(\vec{r}, \theta, \phi) d\Omega \quad (\text{A-1})$$

where $\omega(\vec{r}, \theta, \phi)$ is the light (lumens/steradian-unit area) incident on the volume element from a direction θ, ϕ . The direction $\theta=0$ corresponds to light incident along the +z axis and hence toward the observer. On the right hand side of Eq. A-1, the first term arises from the attenuation of the light already traveling toward the observer, the second term corresponds to scattering of the incident solar radiation, and the third term to the scattering of the diffuse light incident on the volume element from the surrounding regions of the haze. The flux in the incident beam is πF , and τ_s is the optical thickness along the path of the sunlight to the point χ .

$\beta(\vec{r}, \theta)$ is the fraction of the incident light in a unit solid angle that is scattered into a unit solid angle centered at an angle θ to the initial direction, per unit length in the haze. The quantity $b(\vec{r})$ is the fraction of an incident beam which is scattered, regardless of direction, per unit length. In the case of isotropic scattering,

$$b = 4\pi\beta \quad . \quad (A-2)$$

For the second term in Eq. A-1, we require the fraction of light scattered per unit solid angle in the direction of the observer. Since isotropic scattering has been assumed, the result is $b/4\pi$.

The approximation made for first-order scattering is simply to neglect the contributions from the third term in Eq. A-1. The equation becomes

$$\frac{d\omega_1}{d\chi} = -\sigma(\vec{r}) \omega_1(\vec{r}, 0, 0) + \frac{b(\vec{r}) Fe^{-\tau s}}{4} \quad (A-3)$$

where the subscript 1 has been appended to indicate first-order theory. Higher order approximations may be obtained by using the first-order brightness to calculate the integral in Eq. A-1, as follows.

$$\frac{d\omega_2}{d\chi} = -\sigma(\vec{r}) \omega_2(\vec{r}, 0, 0) + \frac{b(\vec{r}) Fe^{-\tau s}}{4} + \int \beta(\vec{r}, \theta) \omega_1(\vec{r}, \theta, \phi) d\Omega \quad (A-4)$$

It is clear that in the foregoing equation, it is necessary to have calculated $\omega_1(\vec{r}, \theta, \phi)$ for all directions at the point χ , and not just along the line of sight. It is possible to repeat the iterative procedure to obtain increased accuracy in the solution.

For the first order theory of the haze, Eq. A-3 has been numerically solved with the assistance of a digital computer. In all of the calculated cases, the observer was taken to be outside the atmosphere, and his line of sight either intersected the planet surface or passed above the limb and continued indefinitely. In the former case, the integration began at the surface, where the initial value was determined by the surface brightness, and proceeded to the observer. In the case where the line of sight passed above the limb, the integration began where the line of sight exceeded the maximum height of the atmosphere (h_{\max}) and proceeded through the atmosphere to the observer. The initial value for the solution was zero.

Finally, the brightness units used throughout the report have been referenced to the brightness of an ideal Lambert surface. For an incident flux πF , the Lambert surface brightness is F . Let us define

$$u = \omega/F \quad (A-5)$$

Then, by dividing through Eq. A-3 by F , we obtain

$$\frac{du}{d\chi} = -\sigma(\vec{r})u + \frac{b}{4} e^{-\tau s} \quad (A-6)$$

which may be compared with Eqs. 4 and 5.

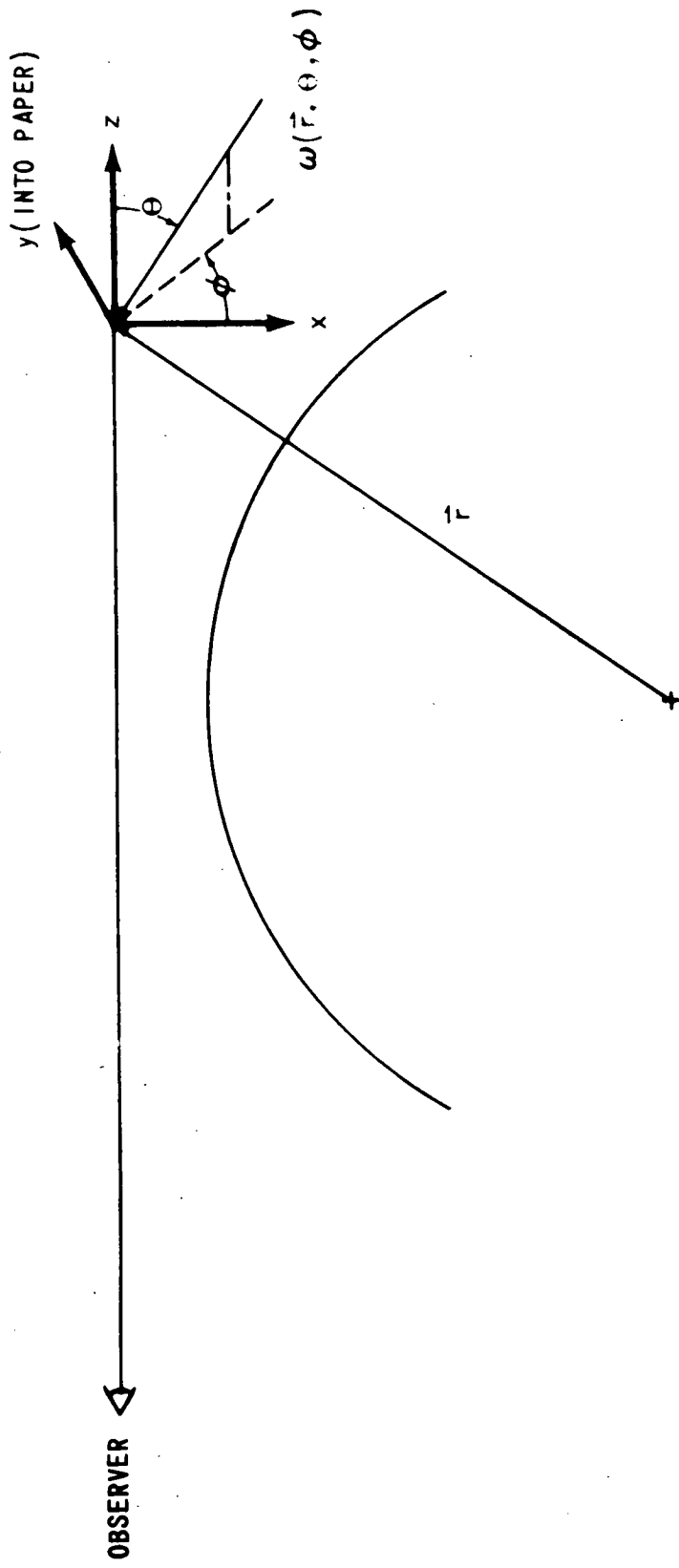


FIGURE A-1 - COORDINATE SYSTEM FOR BRIGHTNESS CALCULATIONS

APPENDIX B

MULTIPLE SCATTERING CALCULATIONSA. Chandrasekhar's Procedure

Chandrasekhar⁽⁴⁾ developed a method of calculating exactly the transfer of light through an atmosphere. His method is applicable to a flat atmosphere of arbitrary thickness. The optical thickness, τ_1 , of the atmosphere is defined by

$$\tau_1 = \int \sigma dh \quad (\text{B-1})$$

where the integral is calculated along a line normal to the plane of the atmosphere. The quantity σ is the extinction coefficient.

The geometry for Chandrasekhar's calculations is shown in Figure B-1. The notation used by Chandrasekhar⁽⁴⁾ is followed in most circumstances. The direction of a beam of light is described by the cosine of the angle between the beam and the upward normal to the atmosphere. The quantity μ refers to the absolute value of the cosine; beams traveling downward have a direction $(-\mu)$. The direction of the incident beam is $(-\mu_0)$. Because of the symmetry inherent in isotropic scattering, with which we will be exclusively concerned, there is no azimuthal dependence for any of the scattered radiation.

The attenuation of a beam of light traveling completely through the atmosphere in a direction $\pm\mu$ may be obtained by solving the differential equation

$$\frac{d\omega}{d\chi} = -\sigma\omega \quad (\text{B-2})$$

Now, if h is measured along the normal to the atmosphere

$$d\chi = dh/\mu \quad (\text{B-3})$$

and the solution of Eq. B-2 may be written

$$\omega = \omega_0 e^{-\tau_1/\mu} \quad (\text{B-4})$$

where ω_0 is the intensity of the beam before entering the atmosphere.

When an incident beam strikes the atmosphere, one may identify three components of emergent radiation. These are the attenuated incident beam which emerges from the bottom of the atmosphere, the diffusely scattered radiation emerging from the top of the atmosphere, and the diffusely transmitted radiation emerging from the bottom of the atmosphere. The term diffuse means that the radiation is not well collimated, in contrast to the incident radiation.

The flux of the incident beam, measured normal to its direction of the propagation, is πF . Then the flux of the attenuated transmitted beam is

$$\pi F e^{-\tau_1/\mu_0} \quad (\text{B-5})$$

The diffusely scattered components of the emergent radiation are given by

$$I(\tau=0, \mu) = \frac{F}{4\mu} S(\tau_1; \mu, \mu_0) \quad (\text{B-6})$$

for the radiation emerging from the top of the atmosphere and by

$$I(\tau=\tau_1; -\mu) = \frac{F}{4\mu} T(\tau_1; \mu, \mu_0) \quad (\text{B-7})$$

for that emerging from the bottom of the atmosphere.

The scattering function and the transmission function, $S(\tau_1; \mu, \mu_0)$ and $T(\tau_1; \mu, \mu_0)$, respectively, are defined in terms of the X and Y functions of Chandrasekhar

$$\left(\frac{1}{\mu_0} + \frac{1}{\mu} \right) S(\tau_1; \mu, \mu_0) = \rho_s \{ X(\mu)X(\mu_0) - Y(\mu)Y(\mu_0) \} \quad (\text{B-8})$$

$$\left(\frac{1}{\mu_0} - \frac{1}{\mu} \right) T(\tau_1; \mu, \mu_0) = \rho_s \{ Y(\mu)X(\mu_0) - X(\mu)Y(\mu_0) \} \quad (\text{B-9})$$

The X and Y functions themselves are dependent on ρ_s , the albedo for single particle scattering, on the optical thickness, τ_1 , of the atmosphere slab and on the scattering law for the atmosphere. The X and Y functions are shown in Figure B-2. The values were obtained from the tabulation of Carlstedt and Mullikin. ⁽⁹⁾

B. Extension to Include a Planetary Surface

The problem which is of concern here includes a slab atmosphere overlaying a Lambert planetary surface. The geometry is shown in Figure B-3.

The total illumination of the surface is defined to be πG . It consists of three parts: the attenuated direct light from the incident beam, light diffusely scattered through the atmosphere, and the light from the surface itself, diffusely scattered back onto the surface. The first two terms are straightforward, but the third term requires some consideration. It requires a double integration, the first to integrate over all directions from which light is scattered back from the atmosphere onto the surface, and the second to integrate over all directions from which light from the surface is incident on the underside of the atmosphere. We write

$$\pi G = \pi G_d + \pi G_t + \pi G_b \quad (B-10)$$

where the terms on the right are, respectively, the illumination from the direct beam, the diffusely transmitted light and the back scattered light. A factor of π is included in each term in conformity with standard notation. It may be straightforwardly shown

$$\pi G_d = \mu_0 \pi F e^{-\tau_1/\mu_0} \quad (B-11a)$$

$$\pi G_t = \left(\frac{\pi F}{2} \right) \int_0^1 T(\tau_1; \mu, \mu_0) d\mu \quad (B-11b)$$

$$\pi G_b = \pi \rho G \int_0^1 d\mu' \int_0^1 d\mu S(\tau_1; \mu, \mu') \quad (B-11c)$$

where ρ is the normal albedo of the planetary surface. Eq. B-10 and B-11 together can be solved for G , the total flux incident on the planet surface.

The observed brightness above the atmosphere is similarly the sum of three terms: diffusely scattered light from the incident beam, attenuated light direct from the surface, and diffusely transmitted light from the surface. These are called, respectively, I_s , I_d and I_t . We have

$$I(\tau=0, \mu) = I_s(\mu) + I_d(\mu) + I_t(\mu) \quad (B-12)$$

and it may be shown

$$I_s(\mu) = \frac{F}{4\mu} S(\tau_1; \mu, \mu_0) \quad (\text{B-13a})$$

$$I_d(\mu) = \rho G e^{-\tau_1/\mu} \quad (\text{B-13b})$$

$$I_t(\mu) = \frac{\rho G}{2\mu} \int_0^1 T(\tau_1; \mu, \mu') d\mu' \quad (\text{B-13c})$$

C. Numerical Results

The integrals contained in Eq. B-11 and B-13 were evaluated through numerical integration on a digital computer.

Because of the reciprocity relationship,

$$T(\tau_1; \mu, \mu_0) = T(\tau_1; \mu_0, \mu) \quad (\text{B-14})$$

the integrals in Eq. B-11b and B-13c are equal. However, the integrand

$$T(\tau_1; \mu, \mu_0) = \frac{\mu \mu_0}{\mu - \mu_0} \rho_s \{Y(\mu)X(\mu_0) - Y(\mu_0)X(\mu)\} \quad (\text{B-15})$$

is singular at $\mu = \mu_0$, and the principal value of the integral must be used.

The accuracy of the entire multiple scattering calculations was checked for the special case where the normal albedo of the surface and the albedo for single scattering were both equal to unity. In this case there is no absorption either in the atmosphere or upon reflection from the surface. The intensity above the atmosphere, integrated over all directions, must equal the flux in the incident beam. The calculated emergent intensity was numerically integrated by the same program used to calculate the integrals in Eq. B-11 and B-13. The total emergent flux agreed with the incident flux to better than 1/2%.

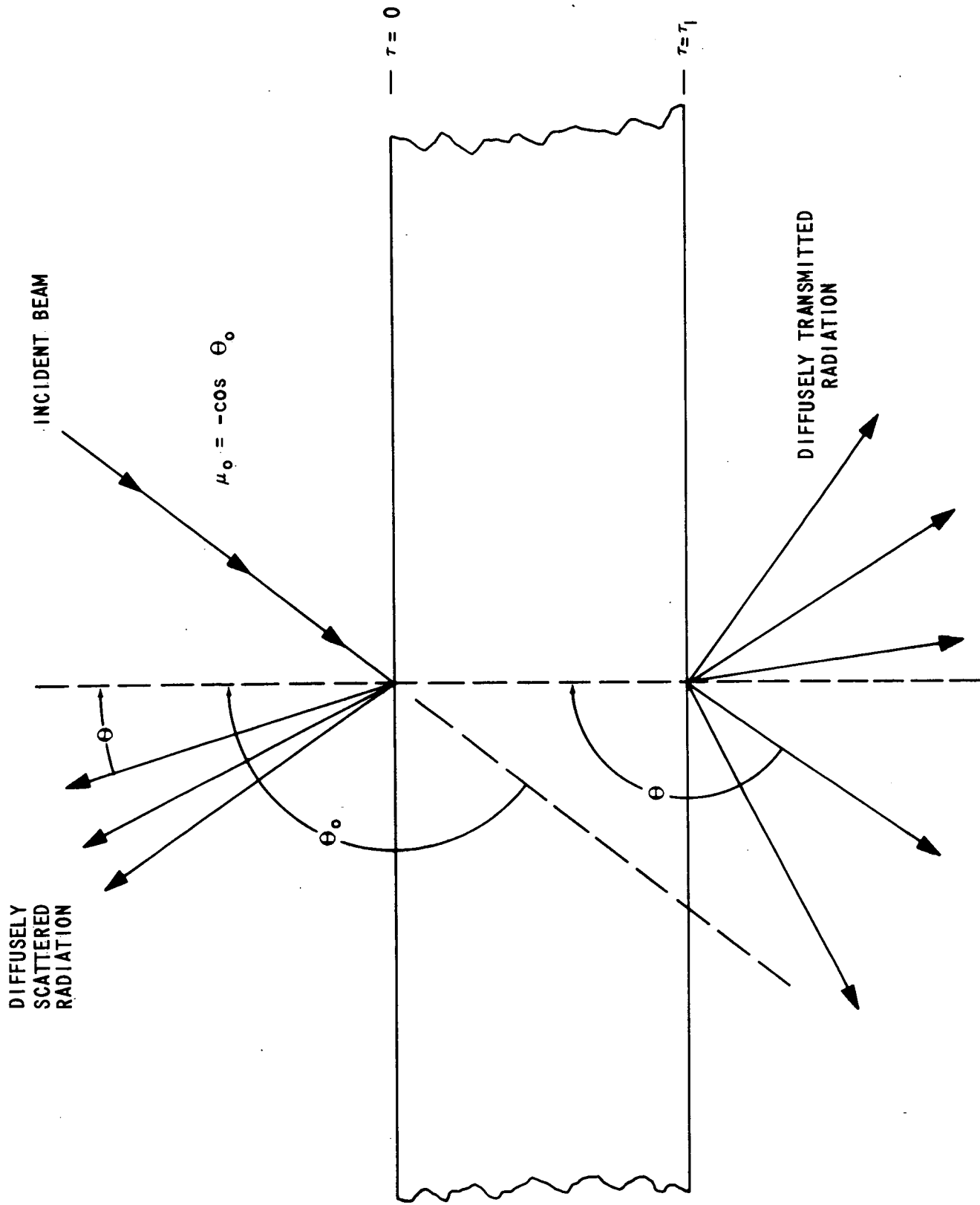


FIGURE B-1 - GEOMETRY FOR CHANDRASEKHAR'S CALCULATIONS.

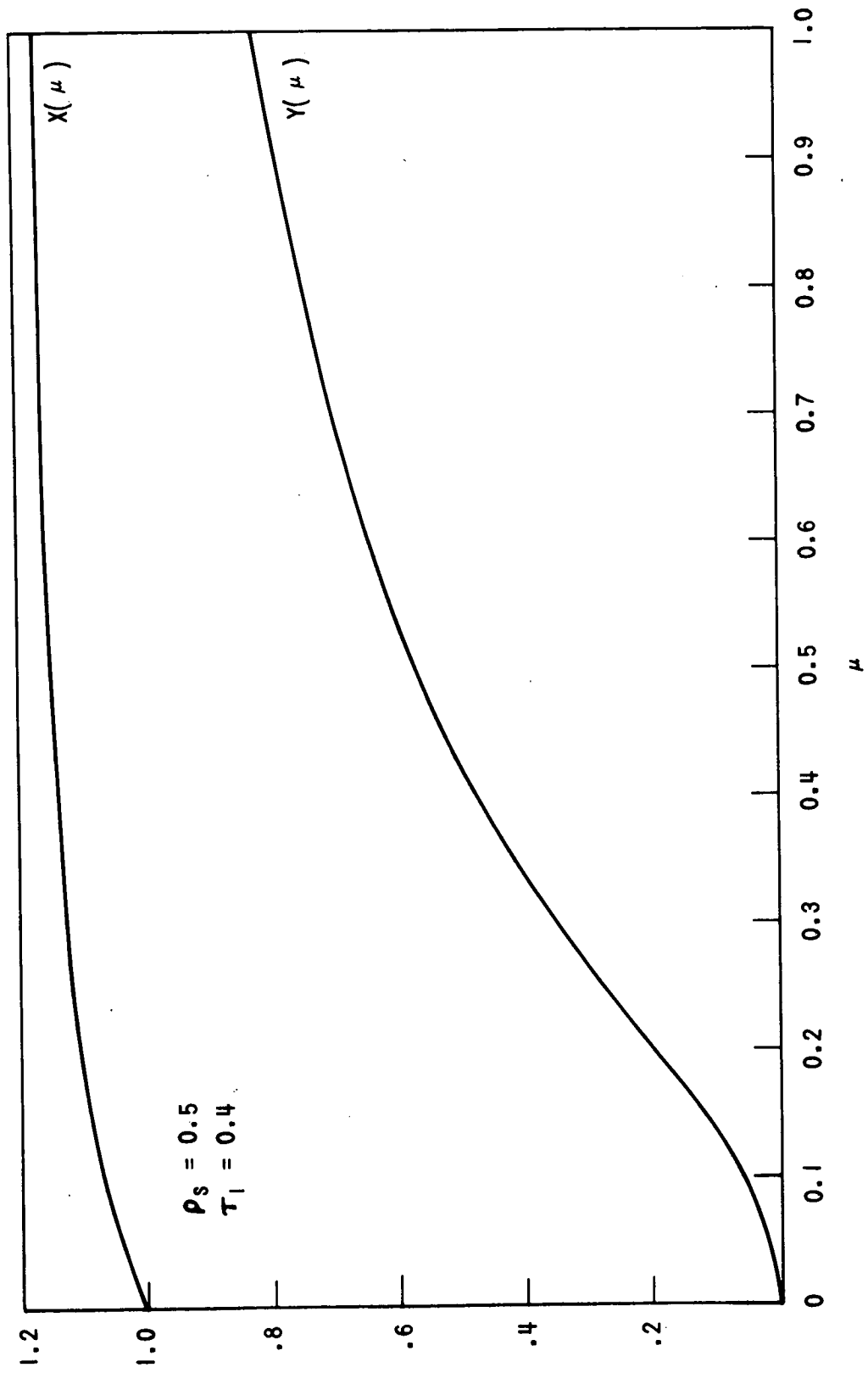


FIGURE B-2 - VALUES OF THE X AND Y FUNCTIONS.

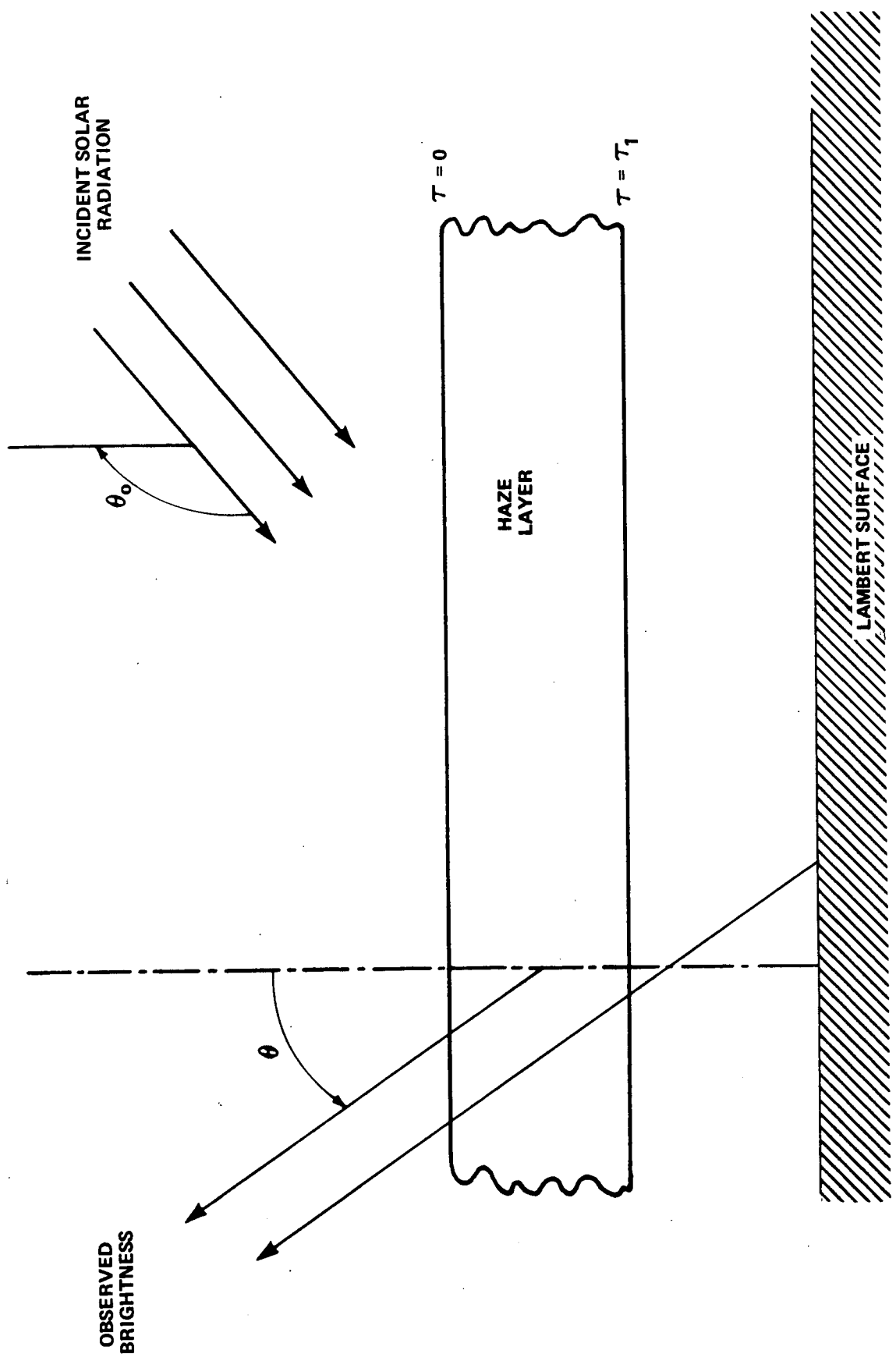


FIGURE B-3 - GEOMETRY FOR THE MULTIPLE SCATTERING CALCULATIONS

Bellcomm, Inc.

DISTRIBUTION LIST

NASA Headquarters

W. O. Armstrong/MTX
N. W. Cunningham/SL
E. W. Glahn/SL
E. W. Hall/MTG
H. F. Hipsher/SL
W. Jakobowski/SL
T. A. Keegan/MA
R. L. Lohman/MTY
D. R. Lord/MTD
D. G. Rea/SL
A. D. Schnyer/MTV
M. G. Waugh/MTP
J. W. Wild/MTE

NASA Headquarters Library (USS-10) (2)

Ames Research Center

L. Roberts/M (2)

Goddard Space Flight Center

R. A. Hanel/620
C. Stephanides/620

Jet Propulsion Laboratory

R. A. Becker/323
S. Z. Gunter/329
A. J. Kliore/311
J. Lorell/311
J. A. Stallkamp/241
R. H. Steinbacher/32
A. T. Young/323

Langley Research Center

G. A. Soffen
I. Taback/159
A. T. Young/159

Manned Spacecraft Center

C. R. Hicks/FA4

California Institute of Technology

N. H. Horowitz
R. B. Leighton
B. C. Murray
G. Neugebauer
R. P. Sharp

Cornell

J. B. Pollack
C. Sagan

Massachusetts Institute of Technology

T. B. McCord
I. I. Shapiro

New Mexico State University

B. Smith

Rand Corporation

M. E. Davies

Stanford University School of Medicine

J. Lederberg
E. Levinthal

University of Arizona

W. K. Hartman

University of Colorado

C. A. Barth

University of Texas

G. de Vaucouleurs

University of Washington

C. Leovy

USGS - Flagstaff, Arizona

R. M. Batson
W. T. Borgeson
H. Masursky
R. L. Wildey

USGS - Menlo Park, California

M. H. Carr
J. F. McCauley
D. J. Milton
D. E. Wilhelms

← COPY TO

Bellcomm, Inc.

DISTRIBUTION LIST (CONT'D)

Bellcomm, Inc.

F. G. Allen
G. M. Anderson
G. C. Bill
A. P. Boysen, Jr.
C. L. Davis
D. A. DeGraaf
D. R. Hagner
C. M. Harrison
N. W. Hanners
B. T. Howard
D. B. James
J. Kranton
H. S. London
K. E. Martersteck
R. K. McFarland
J. Z. Menard
G. T. Orrok
I. M. Ross
F. N. Schmidt
R. V. Sperry
C. M. Thomas
W. B. Thompson
J. W. Timko
R. L. Wagner
J. E. Waldo
All members Division 101
Center 10
Central Files
Department 1024 File
Library